Research Square

Preprints are preliminary reports that have not undergone peer review.
They should not be considered conclusive, used to inform clinical practice,
or referenced by the media as validated information.

Free vibration characteristics of bio-inspired rotating twisted stiffened cylindrical panels with Von-Karman nonlinear effect

Pabitra Maji

pabitrajumech2@gmail.com

Rajiv Gandhi National Aviation University (A Central University

Poonam Kumari

Indian Institute of Technology Guwahati

Bhrigu Nath Singh

Indian Institute of Technology Kharagpur

Research Article

Keywords: Cylindrical shells, Bio-inspired Composite, Vibration, Stiffeners, FEM

Posted Date: May 29th, 2026

DOI: https://doi.org/10.21203/rs.3.rs-9694360/v1

License: This work is licensed under a Creative Commons Attribution 4.0 International License.
Read Full License

Additional Declarations: No competing interests reported.

Free vibration characteristics of bio-inspired rotating twisted stiffened cylindrical panels with Von-Karman nonlinear effect

Pabitra Maji[1*], Poonam Kumari[2], Bhrigu Nath Singh[3]

[1*]Aerospace Engineering, Rajiv Gandhi National Aviation University (A Central University), India.
[2] Department of Mechanical Engineering, Indian Institute of Technology Guwahati, India.
[3] Vice Chancellor, Rajiv Gandhi National Aviation University (A Central University), India & Professor (HAG) on lien, Department of Aerospace Engineering, Indian Institute of Technology Kharagpur, India

Abstract

The bulk of bio-structures that have existed for millions of years in nature, including plants, cartilage, insect wings, and animal bones, have remarkable mechanical qualities due to their distinctive structural and material characteristics. These configurations are used to manufacture the stiffened rotating cylindrical shell. An eight-nodded isoparametric shell bending element is employed to model the geometry of the panels based on the finite element methods incorporated with first-order shear deformation theory. A three-nodded beam element is taken into consideration when modelling the stiffeners. The stiffened panels have more load-carrying capacity than the unstiffened panels, which have the same weight. In this study, seven different types of bio-inspired materials are taken into consideration. Based on Hamilton's principle, the governing equation for free vibration results in bio-inspired composite cylindrical shells derived. Various parametric and convergence studies are performed to check the correctness and precision of the current formulation. Numerous parametric studies are considered in detail, such as the effect of stiffeners, twist angles, pre-cone angles, eccentricity, stiffeners' width, and stiffeners thickness. The first four mode shapes of bio-inspired rotating cylindrical stiffened panels are plotted with stationary conditions and rotational speeds, respectively.

Keywords: Cylindrical shells; Bio-inspired Composite; Vibration; Stiffeners; FEM.

Corresponding authors:
E-mail address: pabitrajumech2@gmail.com (Pabitra Maji)

1 Introduction

The majority of the bio-structures that have been in existence for millions of years in nature, including plants, cartilages, insect wings, and animal bones, exhibit exceptional mechanical properties because of their unique structures and materials properties [1–3]. Many biological systems have extraordinary mechanical properties that are considerably above what can be attained from synthetic materials [3–7]. There are particular and distinctive types of biological materials as shown in **Figure 1**. Biological systems are unique due to their evolution and multifunctionality. Creating these distinct materials and structures from synthetic materials requires more research [8]. The bio-inspired dactyl club influences these structural configurations. The technique of examining the features of biological animals and applying those ideas to engineering buildings is known as bio-inspired design. Thus, the phrase "bio-inspire" refers to the idea of taking inspiration from biological systems, processes, or structures found in nature to address human issues, design technology, or develop novel solutions.

In the twenty-first century, composite materials are increasingly utilised across various sectors, including Mechanical, Aerospace, Automotive, Missiles, Naval Architecture, Nuclear, and Ocean applications, owing to their superior stiffness, strength, thermal and moisture resistance, low specific weight, enhanced damping, and shock absorption capabilities. The stiffener is basically secondary beams or sections like structures attached on one side or on both sides of the panels to increase the dynamic performance characteristics of the shells. It is observed that the stiffened panels have more load-carrying ability compared to unstiffened panels having the same weight. Various sections are usually considered to model the stiffeners, such as flat, I-section, T-section, Z-section, etc. The applications of various stiffened plate elements are found in numerous areas. These kinds of structures may be subjected to various loads such as static, dynamics and impact, etc.

The rotating structures are generally made of composite materials and may be subjected to various loads. Rotor blades of aircraft can be idealised as a low thickness ratio of twisted cylindrical shells. Their curvature enables them to successfully support externally imposed loads despite the geometry of the shell thin. The vibration of rotor blades is directly associated with their frequency values. It is essential to understand their vibration properties to guarantee safe functioning under dynamic loadings. It is very important to find out the actual modal responses behaviour of these structures.

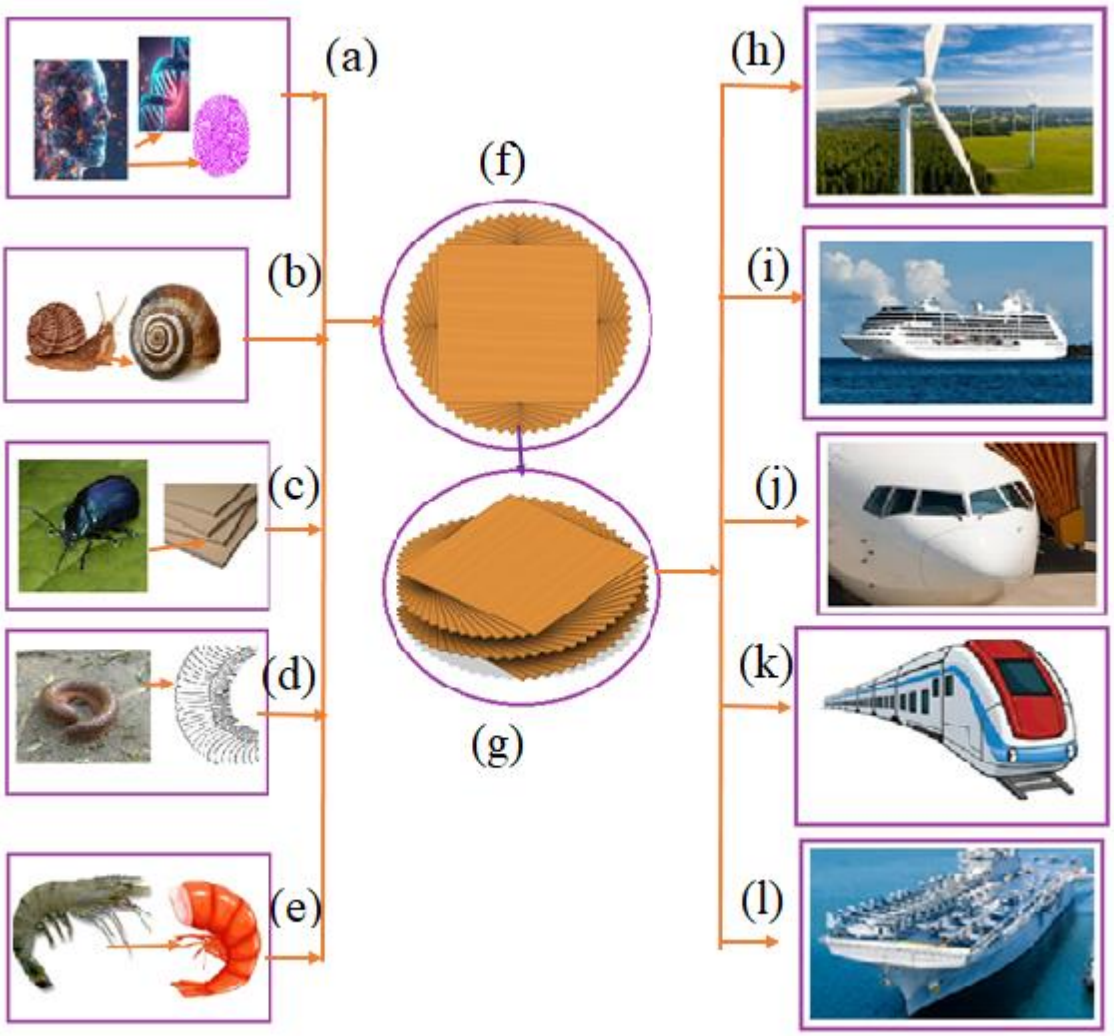


Figure 1: Several helicoidal structures detected macroscopically or microscopically from natural animals, such as (a) DNA and fingerprint of the human body, (b) Snail shell, (c) exoskeleton of beetle (green laminates), (d) exotic millipede (e) carapace from prawn. (f) helicoidal structure biologically motivated by (a)–(e) utilised to design (g) helicoidal laminated composite. Possible bio-inspired composite applications include (h) wind turbine blades, (i) ships, (j) aircraft, (k) high-speed train parts, and (l) aircraft carriers.

Nayak and Bandyopadhyay [9] performed the modal investigation of stiffened shells using the finite element method (FEM) made of laminated composite, where two X and Y- and Y-directional stiffeners are utilised. Sahoo [10] studied the free vibration response of the laminated stiffened spherical shell panels using the finite element method based on first-order shear deformation theory (FSDT). Maji et al. [11] also considered the modal behaviour of graphene-reinforced stiffened plate based on the FEM in the thermal environments. Mouthanna et al. [12] utilized the analytical method to exercise the free vibration behaviour of eccentrically stiffened cylindrical shell panels made of temperature dependent functionally

graded materials. Zhou et al. [13] investigated the modal response of both stringers and rings stiffened composite multilayer cylindrical panels based on the FSDT made of functionally graded graphene nanoplatelet (GPL)-reinforced. Maji et al.[14] also measured the vibration behaviour of carbon nanotube-reinforced stiffened plate based on the FEM in the thermal environments. Duc [15] explored the dynamic characteristics of eccentrically stiffened functionally graded double-curved shallow shells that were resting on elastic foundations using classical shell theory. Using first-order shear deformation theory (FSDT), Yang et al. [16] analysed the acoustic vibration behaviour of stiffened laminated cylindrical shells. They utilised the orthogonal stiffeners to strengthen the cylindrical shells and solved the numerical problems based on the semi-analytical approach. Gao et al.[17] also analysed the acoustic vibration behaviour of stiffened laminated cylindrical shells. They used the ring stiffeners to strengthen the cylindrical shells and solved the numerical problems based on the multi-segment technique.

Reddy and Liu [18] conducted the vibration response of the laminated cylindrical panels using finite element method (FEM) by varying curvature ratios. The shell panels are modelled based on the first-order shear theory. Karmakar and Kishimoto [19], Sreenivasamurthy and Ramamurti [20] studied the vibration characteristics of rotating pre-twisted plate and shell panels based on the FEM. The effect of rotational speeds is discussed in detail by excluding the Coriolis effect. Qatu and Leissa [21] worked out the modal response of the laminated plate with the effect of twist angle. Guo et al. [22] used the linear expression method (LEM) to perform the vibration behaviour of combined conical–cylindrical–spherical shell panels made of composite materials. Jahanbazi et al. [23] used the Ritz method to examine the vibration behaviour of the functionally graded graphene-reinforced skew cylindrical shells using Chebyshev polynomials. Maji et al. [24–27] studied the vibration characteristics of rotating pre-twisted shell panels under the cantilever boundary conditions. They solved the numerical problems using the FEM, where various curved shell panels were considered, including cylindrical and conical shells. Rout et al. [28] conducted the vibration response of the laminated cylindrical stiffened curved panels using finite element method (FEM). The shell panels are modelled based on the first-order shear theory and also explained the effect of rotational speeds and twist angles.

Zhang et al. [29] investigated the vibration behaviour of bio-inspired composite plates made of functionally graded materials (FGM) using the extended finite element method (XFEM). Dhari et al. [30] explored the impact characteristics of bio-inspired Fibonacci laminated composites based on numerical simulations. Mohamed et al.[31] examined the bucking and vibration

behaviour of bio-inspired composite plates based on the first-order shear deformation theory (FSDT). Based on numerical simulations, Ouyang et al. [32] reported the low-velocity impact behaviour of bio-inspired composite plates with varying orientation angles. Do et al. [33] performed a bio-inspired composite plate's modal response on the elastic foundation, employing isogeometric analysis. Garg and Sharma [34] studied the free vibration behaviour of bio-inspired composite plates. In this study, they used the double- and cross-helicoidal lamina sequence. Sharma et al. [4] studied the bending characteristics of bio-inspired laminated composite plates by varying Bouligand lamina sequences using higher-order shear deformation theory. Kiran et al. [35] examined bio-inspired plates' modal and buckling response using the inverse hyperbolic shear deformation theory. They discovered that bio-inspired helicoidal laminates with reduced fibre rotation outperformed conventional composite laminates regarding mechanical properties. Aragh et al. [36] conducted the buckling behaviour of bio-inspired nanocomposite cylindrical shells using FEM.

Tou et al. [3] exhibited the tensile mechanical properties of the fresh and dried forewings. In this study, the authors used two kinds of beetles and reported that these kinds of materials are significantly helpful for bio-metric and other relevant applications. Bouligand-like structures may be found in many organisms, including the mantis shrimp. Silvestre and Pinho [37] examined the damage behaviour of CFRP-based biological Bouligand structures under low-velocity impact. Eltaher et al. [38] revealed the modal and bending response of plates made of bio-inspired laminated composite using numerical methods. The geometry of the bio-inspired plate incorporates the first-order shear deformation theory. Garg and Li [39] conducted a free vibration investigation of helicoidal laminated cylindrical based on numerical simulations. They also scrutinised the uncertainty quantification using data-driven models. Using higher-order FEM models, Karamanli et al. [40] explored the bending, buckling, and vibration response of bio-inspired laminated composite plates. They also compared the present results with the classical composites. Thu et al. [41] recently conducted the dynamic test under blast loads of the bio-inspired doubly curved panels using an isomorphic method. The shell panels are modelled based on the modified first-order shear theory. Daniel and Sudhagar [42] examined the Vibration characteristics of a rotating beam made of bio-inspired laminated composites. Recently, Tao et al. [43] scrutinised the dynamic behaviour of bio-inspired laminated Structures under low-velocity impact.

In the last few decades, most of the investigations carried out were based on the unstiffened shell structure with or without rotation, but few researchers have focused on the modal analysis of bio-inspired rotating stiffened cylindrical panels. To the best of the authors' knowledge, there

is a need for additional research, notably in the realm of bio-inspired rotating stiffened cylindrical panels. To fill this apparent void, the first-order shear deformation theory (FSDT) used to investigate the free vibration response of bio-inspired rotating stiffened cylindrical panels. In the process of modelling the stiffener, three nodded curved isoparametric beam elements are utilised. These stiffened elements have four degrees of freedom, including two translations and rotations. The bio-inspired composites exhibit exceptional mechanical properties because of their unique structures and materials properties. Many biological systems have extraordinary mechanical properties that are considerably above what can be attained from synthetic materials. In this present analysis, the bio-inspired rotating stiffened cylindrical panels are made of bio-inspired synthetic materials. This is the real-life application of wind turbine blades. The finite element code is developed to solve numerical results of the free vibration characteristic of bio-inspired stiffened composite rotating cylindrical shells. The free vibration problems are solved using MATLAB software. In this investigation, the new numerical findings are presented in detail. Identifying the influence of geometric parameters on the natural frequency, such as the number of stiffeners, stiffeners' width and thickness, positions of stiffeners, and curvature effect. The other important parameters, like the effect of rotational speeds, twist angles and pre-cone angles on the natural frequencies of the bio-inspired rotating cylindrical stiffened panels, are addressed in detail. The first four mode shapes of bio-inspired rotating cylindrical stiffened panels are also plotted with stationary conditions and with rotational speeds, respectively.

2 Mathematical formulations

2.1 Geometry of the panels

Bio-inspired rotating stiffened cylindrical panels with the principal radius of curvature along x and y directions, R_x and R_y, respectively, are illustrated in **Figure 2**. In the bio-inspired rotating stiffened cylindrical panels, the radius of curvatures are $R=R_y$, $R_x=\infty$. The geometry of the bio-inspired rotating stiffened cylindrical panels is modelled based on the first-order shear deformation theory (FSDT). The middle plane of the shell is considered to be the reference plane with respect to the local co-ordinate system.

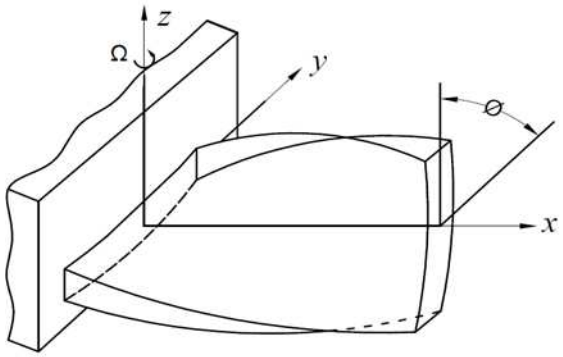


Figure 2: Schematics diagram of bio-inspired rotating stiffened cylindrical panels.

$$u(x,y,z) = u^0(x,y) + z\theta_x(x,y) \tag{1}$$

$$v(x,y,z) = v^0(x,y) + z\theta_y(x,y) \tag{2}$$

$$w(x,y,z) = w^0(x,y) \tag{3}$$

where the transverse displacement of the mid-plane of the panels is represented by the in-plane displacements u^o, v^o, and $w^{o,}$ respectively. The values of θ_x and θ_y represent the rotation of the x and y axes, respectively.

Bio-inspired rotating stiffened cylindrical panels have the twist angle (ϕ), the length of the shell length (a), and the radius of twist (R_{xy}) correlated as [44],

$$\tan\phi = -\frac{a}{R_{xy}} \tag{4}$$

The infinitesimal strains concerning the bio-inspired rotating stiffened cylindrical panels axes x, y, and z are defined by,

$$\{\varepsilon\} = \{\varepsilon^0\} + z\{k\}. \tag{5}$$

$$\{\varepsilon\}^T = \{\varepsilon^0_{xx} \quad \varepsilon^0_{yy} \quad \varepsilon^0_{xy} \quad \varepsilon^0_{xz} \quad \varepsilon^0_{yz}\}^T + z\{k_{xx} \quad k_{yy} \quad k_{xy} \quad k_{xz} \quad k_{yz}\}^T, \tag{6}$$

$$\begin{Bmatrix} \varepsilon^0_{xx} \\ \varepsilon^0_{yy} \\ \varepsilon^0_{xy} \\ \varepsilon^0_{xz} \\ \varepsilon^0_{yz} \end{Bmatrix} = \begin{bmatrix} \frac{\partial}{\partial x} & 0 & 0 & 0 & 0 \\ 0 & \frac{\partial}{\partial y} & 0 & 0 & 0 \\ \frac{\partial}{\partial y} & \frac{\partial}{\partial x} & \frac{2}{R_{xy}} & 0 & 0 \\ 0 & 0 & \frac{\partial}{\partial x} & 1 & 0 \\ 0 & 0 & \frac{\partial}{\partial y} & 0 & 1 \end{bmatrix} \begin{Bmatrix} u^0 \\ v^0 \\ w^0 \\ \theta_x \\ \theta_y \end{Bmatrix} \tag{7}$$

$$\begin{Bmatrix} k_{xx} \\ k_{yy} \\ k_{xy} \\ k_{xz} \\ k_{yz} \end{Bmatrix} = \begin{bmatrix} \frac{\partial}{\partial x} & 0 \\ 0 & \frac{\partial}{\partial y} \\ \frac{\partial}{\partial y} & \frac{\partial}{\partial x} \\ 0 & 0 \\ 0 & 0 \end{bmatrix} \begin{Bmatrix} \theta_x \\ \theta_y \end{Bmatrix}, \tag{8}$$

The stress-resultant of the bio-inspired rotating stiffened cylindrical panels is specified by,

$$\{\sigma\} = [D]\{\varepsilon\} \tag{9}$$

Where [D] is defined as the elasticity matrix of the bio-inspired rotating stiffened cylindrical panels.

The linear elastic strain energy of the bio-inspired rotating stiffened cylindrical panels element due to the rotational effect is expressed as,

$$U_1 = U_{sh} + U_{rot}, \tag{10}$$

$$U_{sh} = \frac{1}{2}\int \{\varepsilon\}^T [\sigma]\ dv \tag{11}$$

$$\{\varepsilon\} = [B]\{\delta_e\}, \tag{12}$$

where [B] is the strain-displacement matrix.

Again, the strain energy contribution of bio-inspired rotating stiffened cylindrical panels resulting from the initial stresses generated due to rotation is expressed as

$$U_1^{Rot} = \int_{vol} \{\varepsilon'\}^T [\sigma_0] dv \tag{13}$$

ε' are well-defined as the nonlinear strain components and σ_0 denoted the initial stress vector resulting from rotation.

The non-linear strain components of the bio-inspired rotating stiffened cylindrical panels can be written as Cook et al. [45]:

$$\{\varepsilon'\} = \frac{1}{2}\begin{bmatrix} \psi_x^T & 0 & 0 \\ 0 & \psi_y^T & 0 \\ \psi_y^T & \psi_x^T & 0 \\ \psi_z^T & 0 & \psi_x^T \\ 0 & \psi_z^T & \psi_y^T \end{bmatrix} \begin{Bmatrix} \psi_x \\ \psi_y \\ \psi_z \end{Bmatrix} = \frac{1}{2}[A]\{\psi\} \tag{14}$$

$$\left.\begin{aligned}\psi_x^T &= \left[\frac{\partial u}{\partial x}+\frac{w}{R_x},\frac{\partial v}{\partial x}+\frac{w}{R_{xy}},\frac{\partial w}{\partial x}-\frac{u}{R_x}\right]\\ \psi_y^T &= \left[\frac{\partial u}{\partial y}+\frac{w}{R_{xy}},\frac{\partial v}{\partial y}+\frac{w}{R_y},\frac{\partial w}{\partial y}-\frac{v}{R_y}\right]\\ \psi_z^T &= \left[\frac{\partial u}{\partial z},\frac{\partial v}{\partial z},\frac{\partial w}{\partial z}\right]\end{aligned}\right\} \tag{15}$$

$$\text{or } \{\psi\} = [G]\{\delta_c\} \tag{16}$$

[G] Represents the matrix of the derivatives of the shape functions.

where, the matrix $[G]$ consists of derivatives of shape functions and $[M_\sigma]$ denotes the matrix of initial stresses. The strain energy of the bio-inspired rotating stiffened cylindrical panels becomes:

$$\begin{aligned}U_1^{Rot} &= \frac{1}{2}\int_A \{\delta_e\}^T [G]^T [M_\sigma][G]\{\delta_e\}dxdy\\ &= \frac{1}{2}\{\delta_e\}^T [K_{\sigma e}]\{\delta_e\}\end{aligned} \tag{17}$$

where, the element geometric stiffness matrix is defined as:

$$[K_{\sigma e}] = \int_A [G]^T [M_\sigma][G]dxdy \tag{18}$$

Finally, the total strain energy of the bio-inspired rotating stiffened cylindrical panels is written as,

$$U_1 = \frac{1}{2}\{\delta_e\}^T [K_e]\{\delta_e\} + \frac{1}{2}\{\delta_e\}^T [K_{\sigma e}]\{\delta_e\} \tag{19}$$

The elemental elastic stiffness matrix of bio-inspired rotating stiffened cylindrical panels is denoted as

$$[K_{se}] = \int_A [B]^T [D][B]dA \tag{20}$$

The elemental elastic mass matrix of stiffened doubly curved panels is denoted as,

$$[M_{se}] = \int_A [N]^T [m][N]dA \tag{21}$$

2.2 The kinetic energy of the composite stiffened shell panel

The kinetic energy U_2 of composite stiffened shell panel in terms of the velocity at a point in the system as

$$U_2 = \frac{1}{2}\int_v \rho \vec{V}.\vec{V}\, dv \tag{22}$$

For modelling a composite stiffened shell panel, two different reference coordinate systems i.e. (X', Y', Z') and (x, y, z), are used and shown in **Figure 3**. It is defined as the absolute velocity vector of an arbitrary point on the composite stiffened shell panel relative to an inertial reference frame (X', Y', Z') and ρ is the mass density of the composite shell.

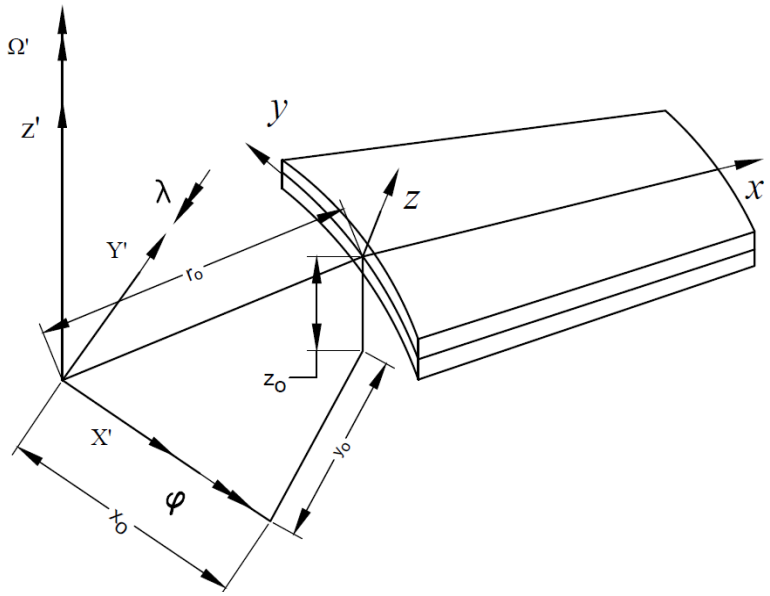


Figure 3: Bio-inspired rotating stiffened cylindrical panels with local and inertial frames of reference.

The Ω' is the speed of rotation of the composite stiffened shell panel about the z-axis of the absolute coordinate system(x', y', z'), λ is defined as precone angle, and χ is defined as skew angle. The order of rotation is χ and λ. The angular velocity components with respect to the composite stiffened shell panel local coordinate system are articulated as [19]

$$\{\Omega'_x, \Omega'_y, \Omega'_z\} = \{0, 0, \Omega'\}[T_{\theta y}]^T [T_{\theta x}]^T \tag{23}$$

The fixed translation offsets of the bio-inspired rotating stiffened cylindrical panels with reference coordinate systems are expressed as,

$$\{h_x, h_y, h_z\} = \{x_0, y_0, z_0\}[T_{\theta y}]^T [T_{\theta x}]^T \tag{24}$$

For the inertial reference system, the unit vectors are (i', j', k') and for the local coordinate axes, they are (i, j, k). Based on the Chasle's theorem, the velocity vector is expressed as,

$$\vec{V} = \frac{d\vec{r}}{dt} + (\Omega' k') X \vec{r} \tag{25}$$

Where, $\vec{r}$ describes the position vector from the origin of the inertial reference frame to a location on the deformed Bioinspired spinning stiffening cylindrical panels. The position vector and angular velocity can be articulated as,

$$\vec{r} = (X_0 + x + u)i + (Y_0 + y + v)j + (Z_0 + z + w)k \tag{26}$$

$$\vec{\Omega}' = \Omega' k' = \Omega'_x i + \Omega'_y j + \Omega'_z k \tag{27}$$

Finally, the Kinetic energy articulated as,

$$\begin{aligned} U_2 = {} & \frac{1}{2}\int_{vol} \rho \begin{Bmatrix} \dot{u} \\ \dot{v} \\ \dot{w} \end{Bmatrix}^T \begin{Bmatrix} \dot{u} \\ \dot{v} \\ \dot{w} \end{Bmatrix} dv + \frac{1}{2}\int_{vol} \rho \begin{Bmatrix} \dot{u} \\ \dot{v} \\ \dot{w} \end{Bmatrix}^T [A_1] \begin{Bmatrix} u \\ v \\ w \end{Bmatrix} dv + \frac{1}{2}\int_{vol} \rho \begin{Bmatrix} u \\ v \\ w \end{Bmatrix} [A_2] \begin{Bmatrix} u \\ v \\ w \end{Bmatrix} dv \\ & + \int_{vol} \rho \begin{Bmatrix} h_x + x \\ h_y + y \\ h_z + z \end{Bmatrix}^T [A_2] \begin{Bmatrix} u \\ v \\ w \end{Bmatrix} dv \end{aligned} \tag{28}$$

Details description of [A_1] and [A_2] are expressed in the Appendix.

Where, [N] denoted the shape function matrix and $\{d_e\}$ denoted the elemental nodal displacement vector and expressed as,

$$\{d\} = [N]\{d_e\}, \text{ where } \{d\} = \{u \quad v \quad w\}^T \tag{29}$$

Substituting the equation (25) in the equation (24), the expression of the kinetic energy of bio-inspired rotating stiffened cylindrical panels becomes,

$$
\begin{aligned}
U_2 &= \frac{1}{2}\int_{vol}\rho\{\dot{\delta}_e\}^T[N_e]^T[N_e]\{\dot{\delta}_e\}\,dv + \frac{1}{2}\int_{vol}\rho\{\dot{\delta}_e\}^T[N_e]^T[A_1][N_e]\{\delta_e\}\,dv \\
&+ \frac{1}{2}\int_{vol}\rho\{\delta_e\}^T[N_e]^T[A_2][N_e]\{\delta_e\}\,dv \\
&+ \int_{vol}\rho\begin{Bmatrix}h_x+x\\ h_y+y\\ h_z+z\end{Bmatrix}^T[A_2][N_e]\{\delta_e\}\,dv \\
&= \frac{1}{2}\{\dot{\delta}_e\}^T[M_e]\{\dot{\delta}_e\} + \frac{1}{2}\{\dot{\delta}_e\}^T[C_e]\{\delta_e\} + \frac{1}{2}\{\delta_e\}^T[K_{rot}]\{\delta_e\} + \{\delta_e\}^T[F_{\Omega e}]
\end{aligned}
\tag{30}
$$

The mass matrix of the bio-inspired rotating stiffened cylindrical panels is written as,

$$
[M_e] = \rho\int_v [N_e]^T[N_e]dv = \int_A [N_e]^T[m][N_e]dxdy \tag{31}
$$

The Coriolis matrix (skew-symmetric) is written as,

$$
[C_e] = \rho\int_v [N_e]^T[A_1][N_e]dv \tag{32}
$$

The rotational stiffness matrix (symmetric and positive definite) is defined as,

$$
[K_{Rot}] = \rho\int_v [N_e]^T[A_2][N_e]dv \tag{33}
$$

The centrifugal force vector is expressed as,

$$
[F_{\Omega e}] = \rho\int_v [N_e]^T[A_2]\begin{Bmatrix}h_x+x\\ h_y+y\\ h_z+z\end{Bmatrix}dv \tag{34}
$$

Where, the dot (.) represents derivative with respect to time.

The total kinetic energy of the bio-inspired rotating stiffened cylindrical panels element is written as,

$$
U_2 = \frac{1}{2}\{\dot{\delta}_e\}^T[M_e]\{\dot{\delta}_e\} + \frac{1}{2}\{\dot{\delta}_e\}^T[C_e]\{\delta_e\} + \frac{1}{2}\{\delta_e\}^T[K_{rot}]\{\delta_e\} + \{\delta_e\}^T[F_{\Omega e}] \tag{35}
$$

2.3 Stiffeners formulations:

In the process of modelling the stiffener, three nodded curved isoparametric beam elements are utilized. These elements have four degrees of freedom, which include two translations and two rotations. For the purpose of the stiffener, a rectangular section composed of graphene-reinforced composite materials with a constant width (b_{st}) and depth (d_{st}) is being evaluated.

The shape functions for the stiffeners that behave in an X-directional direction are expressed as

$$N_i^x = 0.5\xi\xi_i(1+\xi\xi_i) \quad \text{for} \quad i=1,3 \qquad N_i^x = (1-\xi^2) \quad \text{for} \quad i=2$$
$$N_i^y = 0.5\eta\eta_i(1+\eta\eta_i) \quad \text{for} \quad i=1,3 \qquad N_i^y = (1-\eta^2) \quad \text{for} \quad i=2 \tag{36}$$

The nodal degree of freedom of the X-stiffener can be expressed as,

$$\sum_{i=1}^{3}\{\delta_i^{sx}\} = \sum_{i=1}^{3}[T_{sx}]\sum_{j=1}^{8}\begin{bmatrix} N_{ij} & 0 & 0 & 0 & 0 \\ 0 & N_{ij} & 0 & 0 & 0 \\ 0 & 0 & N_{ij} & 0 & 0 \\ 0 & 0 & 0 & N_{ij} & 0 \\ 0 & 0 & 0 & 0 & N_{ij} \end{bmatrix}\begin{Bmatrix} u_j^0 \\ v_j^0 \\ w_j^0 \\ \theta_{xj} \\ \theta_{yj} \end{Bmatrix}. \tag{37}$$

Where, $\{\delta_i^{sx}\} = \{u_0^{sx} \quad w_0^{sx} \quad \theta_0^{sx} \quad \theta_0^{sx}\}^T$ is displacement vector. The eccentricity of the stiffener articulated as,

$$e = \left(\frac{h+d_{st}}{2}\right) \tag{38}$$

The stress-resultant of the X-directional stiffener is given by,

$$[\sigma^{sx}] = [D^{sx}][\varepsilon^{sx}] = [D^{sx}][B^{sx}][\delta_i^{sx}] \tag{39}$$

$$\{\varepsilon^{sx}\} = \left\{\frac{\partial u^{sx}}{\partial x} \quad \frac{\partial \theta^{sx}}{\partial x} \quad \frac{\partial \theta^{sx}}{\partial x} \quad \left(\frac{\partial \theta^{sx}}{\partial x} + \frac{\partial w^{sx}}{\partial x}\right)\right\}^T \tag{40}$$

The X-directional stiffener has an elasticity matrix given by,

$$\left[D^{sx}\right] = \begin{bmatrix} A_{11}^s b_{st} & B_{11}^s b_{st} & B_{16}^s b_{st} & 0 \\ B_{11}^s b_{st} & D_{11}^s b_{st} & D_{16}^s b_{st} & 0 \\ B_{16}^s b_{st} & D_{16}^s b_{st} & \frac{1}{6}(Q_{66}^s + Q_{44}^s) b_{st}^3 d_{st} & 0 \\ 0 & 0 & 0 & S_{44}^s b_{st} \end{bmatrix} \tag{41}$$

$$[A_{ij}^s \quad B_{ij}^s \quad D_{ij}^s] = \sum_{k=1}^{nl}\int_{z_{k-1}}^{z_k}(\overline{Q}_{ij})_k(1, z, z^2)dz \qquad i,j = 1,6 \tag{42}$$

$$[S_{ij}^s] = k_s\sum_{k=1}^{nl}\int_{z_{k-1}}^{z_k}(\overline{Q}_{ij})_k dz \qquad i,j = 4 \tag{43}$$

where A_{ij}^s is defined extension stiffness matrix, B_{ij}^s is defines extension bending coupling matrix, D_{ij}^s is bending stiffness matrix.

2.3.1 Generalized Inertia Matrix

The generalized inertia matrix per unit length of the *X*- directional stiffeners includes both the translator and rotary inertia terms. The mass and moment of inertia are the measures of translator and rotary inertial resistances respectively and are given by the following equations. Mass per unit length of the x-stiffener is denoted by *m* and is given by

$$m_{sx} = \sum_{k=1}^{nlx} b_{st}(z_k - z_{k-1})\rho_k \tag{44}$$

Mass moment of inertia per unit length is denoted by I_{msx} and is given by

$$I_{msx} = \frac{1}{3}\sum_{k=1}^{nlx} b_{st}(z_k^3 - z_{k-1}^3)\rho_k \tag{45}$$

Equivalent mass polar moment of inertia per unit length is denoted by J_{msxe} and given by

$$J_{msxe} = \frac{1}{3}\sum_{k=1}^{nlx} b_{st}(z_k - z_{k-1})\rho_k b_{st}^3 \tag{46}$$

where ρ_k is the mass density of *k*th layer of x-directional stiffener b_{st} and d_{st} are width and depth of the stiffeners, respectively. z_k and z_{k-1} are the distances measured from the mid-surface of stiffener laminate to the bottom of the *k*th and (*k-1*)th laminae.

Incorporating both the translatory and rotary inertia terms the generalized inertia matrix [m^{sx}] of the x-directional stiffeners takes the following form,

$$\left[m^{sx}\right] = \begin{bmatrix} m_{sx} & 0 & 0 & 0 \\ 0 & m_{sx} & 0 & 0 \\ 0 & 0 & I_{msx} & 0 \\ 0 & 0 & 0 & J_{msxe} \end{bmatrix} \tag{47}$$

The elemental elastic stiffness matrix of the stiffeners of the bio-inspired rotating stiffened cylindrical panels is denoted as,

$$[K_{sxe}] = \int_{-1}^{1} [T_{sx}]^T [B_{sx}]^T [D_{sx}][B_{sx}][T_{sx}][J_{sx}]d\xi \tag{48}$$

$$[K_{sye}] = \int_{-1}^{1} [T_{sy}]^T [B_{sy}]^T [D_{sy}][B_{sy}][T_{sy}][J_{sy}]d\eta \tag{49}$$

$$[K_e] = [K_{se}] + [K_{sxe}] + [K_{sye}] \tag{50}$$

The elemental mass matrix of stiffeners of the bio-inspired rotating stiffened cylindrical panels is denoted as,

$$[M_{sxe}] = \int_{-1}^{1} [T_{sx}]^T [N_{sx}]^T [m_{sx}][N_{sx}][T_{sx}][J_{sx}]d\xi \tag{51}$$

$$[M_{sye}] = \int_{-1}^{1} [T_{sy}]^T [N_{sy}]^T [m_{sy}][N_{sy}][T_{sy}][J_{sy}] d\eta \tag{52}$$

$$[M_e] = [M_{se}] + [M_{sxe}] + [M_{sye}] \tag{53}$$

2.4 Solution procedure:

Based on Hamilton's principle, the governing equation for bio-inspired composite plates can be derived as,

$$\int_{t_i}^{t_f} (\delta U_2 - \delta U_1 - \delta U_3) dt = 0 \tag{54}$$

Where U_2, U_1, and U_3 are stated as kinetic energy, strain energy, and external work done. Without taking into account the results of the damping and Coriolis effect, The equation of motion for the analysis of free vibrations is provided as [45],

$$[M_e]\{\ddot{d}_e\} + ([K_e] + [K_{\sigma e}])\{d_e\} = 0 \tag{55}$$

The total stiffness [K] and mass [M] matrices of the bio-inspired rotating stiffened cylindrical panels are computed bellow,

$$[K] = \sum_{i=1}^{ne} [K_e], \; [K_\sigma^{th}] = \sum_{i=1}^{ne} [K_{\sigma e}^{th}], \text{ and } [M] = \sum_{i=1}^{ne} [M_e] \tag{56}$$

Equations of free vibration in the global system of the bio-inspired rotating stiffened cylindrical panels are obtained by [28],

$$[M]\{\ddot{d}\} + ([K] + [K_\sigma^{th}])\{d\} = 0 \tag{57}$$

For the harmonic vibrations, $\{d\} = \{d\}e^{i\omega_n t}$, we have

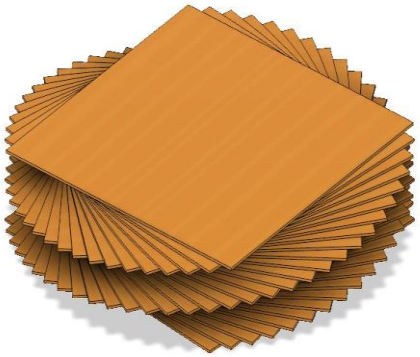
$$[([K] + [K_\sigma^{th}]) - \omega_n^2 [M]]\{d\} = 0 \tag{58}$$

The solution to this problem is found for both the eigenvalue and the eigenvectors. This is a standard eigenvalue problem. [46],

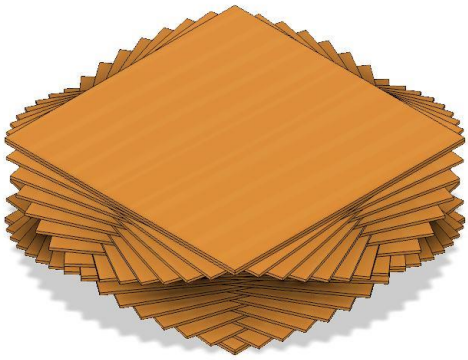
$$[A]\{d\} = \lambda\{d\} \tag{59}$$

Where, $[A] = ([K] + [K_\sigma^{th}])^{-1}[M]$ and $\lambda = 1/\omega_n^2$

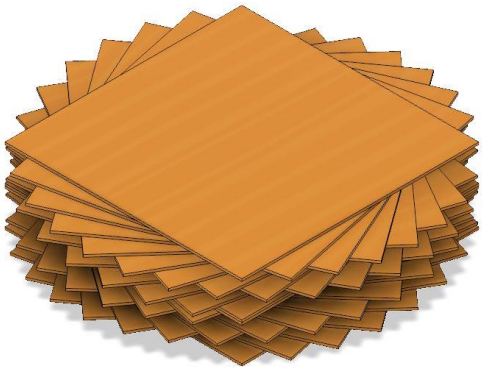
2.4.1 Geometric configurations of bio-inspired composites.



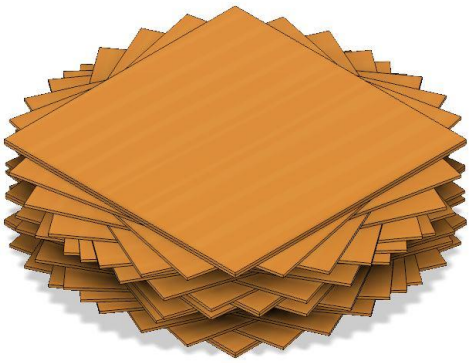
(a) Double-Helicoidal 6◦ (DH6)



(b) Cross-Helicoidal 6◦ (CH6)



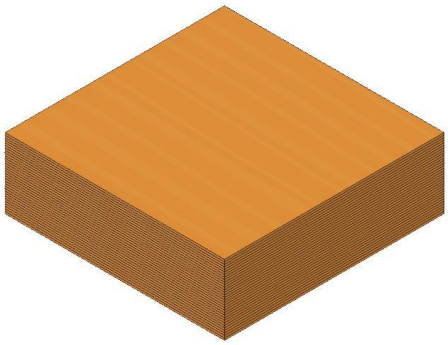
(c) Double-Helicoidal 12◦ (DH12)



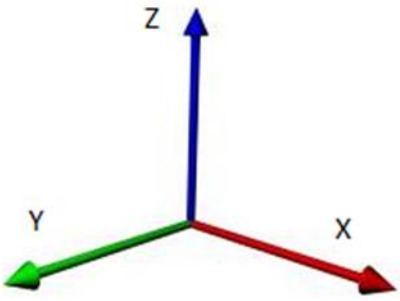
(d) Cross-Helicoidal 12◦ (CH12)

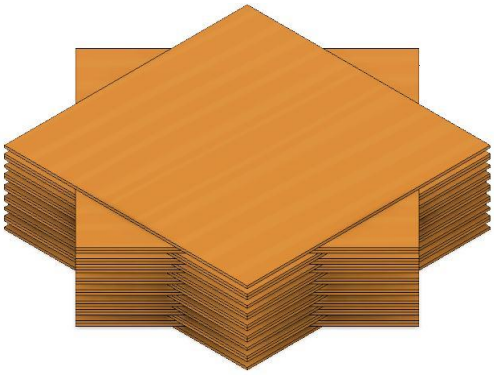


(e) Fibonacci helicoidal (FI)



(f) Cross-ply laminate (CPL)





(g) Quasi-isotropic (QI)

Figure 4: Schematics diagram of Stacking sequences of bio-inspired composites.

Table 1. Stacking sequences of bio-inspired rotating stiffened cylindrical panels.

Sl No	Configuration	Stacking sequence
1	Double-Helicoidal 6◦ (DH6)	[0/6/12/…/84/ 90]s
2	Cross-Helicoidal 6◦ (CH6)	[0/90/6/…/6/90/0]
3	Double-Helicoidal 12◦ (DH12)	[0/12/24/…/168/ 180]s
4	Cross-Helicoidal 12◦ (CH12)	[0/180/12/ …/12/180/..]
5	Fibonacci helicoidal (FI)	$[0/10/10/20\ldots..]_{32}$
6	Cross-Ply (CP)	[0/90]8s
7	Quasi-isotropic (QI)	[0/-45/45/90/0]4s

2.5 Validations:

The finite element code is being developed to offer numerical results with the aim of analysing the free vibration characteristic of bio-inspired stiffened composite rotating cylindrical shells. The vibration results of "eccentric at bottom" stiffeners with simply supported anti-symmetric cross-ply cross-stiffened plates are shown in **Table 2**. It is observed that the results closely resemble those of published results. **Table 2** additionally indicates the examination of convergence of non-dimensional fundamental natural frequencies of laminated stiffened plates, considering 6 x 6, 8 x 8, and 10 x 10 mesh sizes, in that order. For the two mesh sizes (8x8 and 10x10), the results show a percentage difference of less than one, which is nearly equal. In order to obtain the following result, a smaller mesh size of (8x8) has been used to improve computational efficiency. The natural frequencies of the square of an isotropic rotating plate with cantilever boundary conditions are compared in **Table 3** with the reference results of Nayak and Bandyopadhyay [9]. **Table 4** comprises the natural frequencies of twisted plates with different fibre orientation angles. It is clear that the current results match up with those of Qatu and Leissa [21]. The fundamental natural frequencies of square laminated cylindrical shells with curvature ratios are shown in **Table 5**. In **Table 6** displays the validation natural frequency of bio -inspired plate by varying stacking sequence. It is noted that the results closely be similar to those of published results of the literature. The validations listed above have shown that the current formulation is accurate and correct.

Table 2: Fundamental frequencies (Hz) of SSSS-supported stiffened plate made of cross ply.

Mode	Nayak and Bandyopadhyay [9]	Present FEM		
		(6×6)	(8×8)	(10×10)
1	1141.00	1141.83	1141.34	1141.24
2	2394.17	2408.75	2400.85	2398.55
3	2415.82	2425.38	2419.29	2417.61
4	2646.18	2658.33	2651.84	2650.22

Table 3. Non-dimensional fundamental frequencies of rotating cantilever plate made of isotropic material.

Ω	Karmakar and Kishimoto [19]	Sreenivasamurthy and Ramamurti [20]	Present Fem
0.0	3.41969	3.43685	3.41683
0.2	3.49992	3.51858	3.4969
0.4	3.72887	3.75280	3.7256
0.6	4.07813	4.12875	4.0745
0.8	4.51561	4.56786	4.5115
1.0	5.01415	5.09167	5.0096

Table 4: Non-dimensional fundamental frequencies $\varpi = (\omega b^2 / h)\sqrt{\rho / E_2}$ of three layers [$\theta/-\theta/\theta$] cantilever square laminated plate with twisted.

θ	Twist angle 15		30	
	Qatu and Leissa [21]	Present Fem	Qatu and Leissa [21]	Present Fem
0	1.0093	1.00536	0.9617	0.95777
30	0.8299	0.82537	0.8634	0.85903
60	0.6838	0.68115	0.6533	0.65063
90	0.6445	0.64304	0.6142	0.61280

Table 5: Non-dimensional fundamental frequencies $\varpi = (\omega b^2 / h)\sqrt{\rho / E_2}$ of a simply supported (SSSS) laminated cylindrical shell with *a/b*=1.0, *a/h*=100.

R/a	Cylindrical shell		
		$0^0/90^0$	$0^0/90^0/0^0$
5	Present Fem	16.6871	20.3388
	Reddy and Liu [18]	16.690	20.330
10	Present Fem	11.8380	16.6273
	Reddy and Liu [18]	11.840	16.620

Table 6. Non- dimensional natural frequency of the simply supported (SSSS) helicoidal plates with different values of *a/h.*

a/h		DH6	CH6	DH12	CH12	CPL	QI
100	Garg and Sharma [34]	20.8146	19.4591	21.3145	21.3959	18.8703	22.3375
	Present	19.7051	19.4357	20.9977	21.4921	18.8537	22.5050
50	Garg and Sharma [34]	20.5332	19.3102	21.2236	21.1872	18.7537	22.1459
	Present	19.5005	19.2969	20.8165	21.2910	18.7383	22.3115
20	Garg and Sharma [34]	19.0029	18.4277	19.9157	19.8882	17.9972	20.938
	Present	18.3892	18.4514	19.7391	20.0358	17.9888	21.0885

3 Results and discussions:

An eight-noded isoparametric finite element approach is employed to model the geometry of bio-inspired rotating stiffened cylindrical shell panels via first-order shear deformation. To investigate the free vibration behaviour of bio-inspired cylindrical shells with and without a twist angle, the numerical code is constructed with the help of the Matlab program. The crucial geometric constraints for the existing investigates are length (a), width (b), curvature ratios (R_y/a), thickness (h), the principal radius of curvature (R_y), twist angle (ϕ), the effect of stiffeners, the effect of eccentricity and rotational speeds. In the entire investigation, eccentricity at the top (ECB, when e>0), the pre-cone angle (λ=0), and cantilever boundary conditions are assumed.

The boundary conditions (BCs) are utilised for the current study,

For SSSS cases:

x=0, a; $$v_0 = w_0 = \theta_y = 0, \tag{60}$$

y=0, b; $$u_0 = w_0 = \theta_x = 0. \tag{61}$$

For CFFF cases:

x=0; $$u_0 = v_0 = w_0 = \theta_x = \theta_y = 0. \tag{62}$$

3.1.1 Effect of eccentricity (e=(h+ d_{st})/2) and rotational speeds (Ω) :

In the Present parametric study, the natural frequency (FF) of the bio-inspired rotating stiffened cylindrical panels (CYS) are obtained by eccentricity with various stacking sequences. The results are plotted against rotational speed (**Ω**=**Ω**$'$ /ω_n, where ω_n, is denoted static fundamental frequency, **Ω**$'$ is the real rotational speed) and illustrated in **Figure 5**. The parameters are as a/b =1, a/h=20, R_y=10a, b_{st} =h, d_{st} =$2h$, n_x=1, and n_y=1 are kept constant. In this particular example, three different stiffeners are used based on the eccentricity: eccentricity at the top (ECT, when e<0), concentric (COC, when e=0), and eccentricity at the top (ECB, when e>0). Interestingly, the maximum natural frequency values are identified when stiffeners are placed eccentrically at the bottom (ECB) and the minimum when stiffeners are concentric (COC). Therefore, ECB stiffeners are perfect for bio-inspired rotating stiffened cylindrical panels (CYS), providing better results than other stiffeners. Further, it may be well-known that the more effective effect of the stiffeners is observed in DH12 configurations. In contrast, the less effective effect of stiffeners is observed in similar analyses in QI configurations. It is obvious that the FF values of the panels increase with the rise in rotational speeds for all bio-inspired panels for all types of stiffeners. This pattern is evident since the conical shell's structural rigidity consistently increases as the rotational speeds rise.

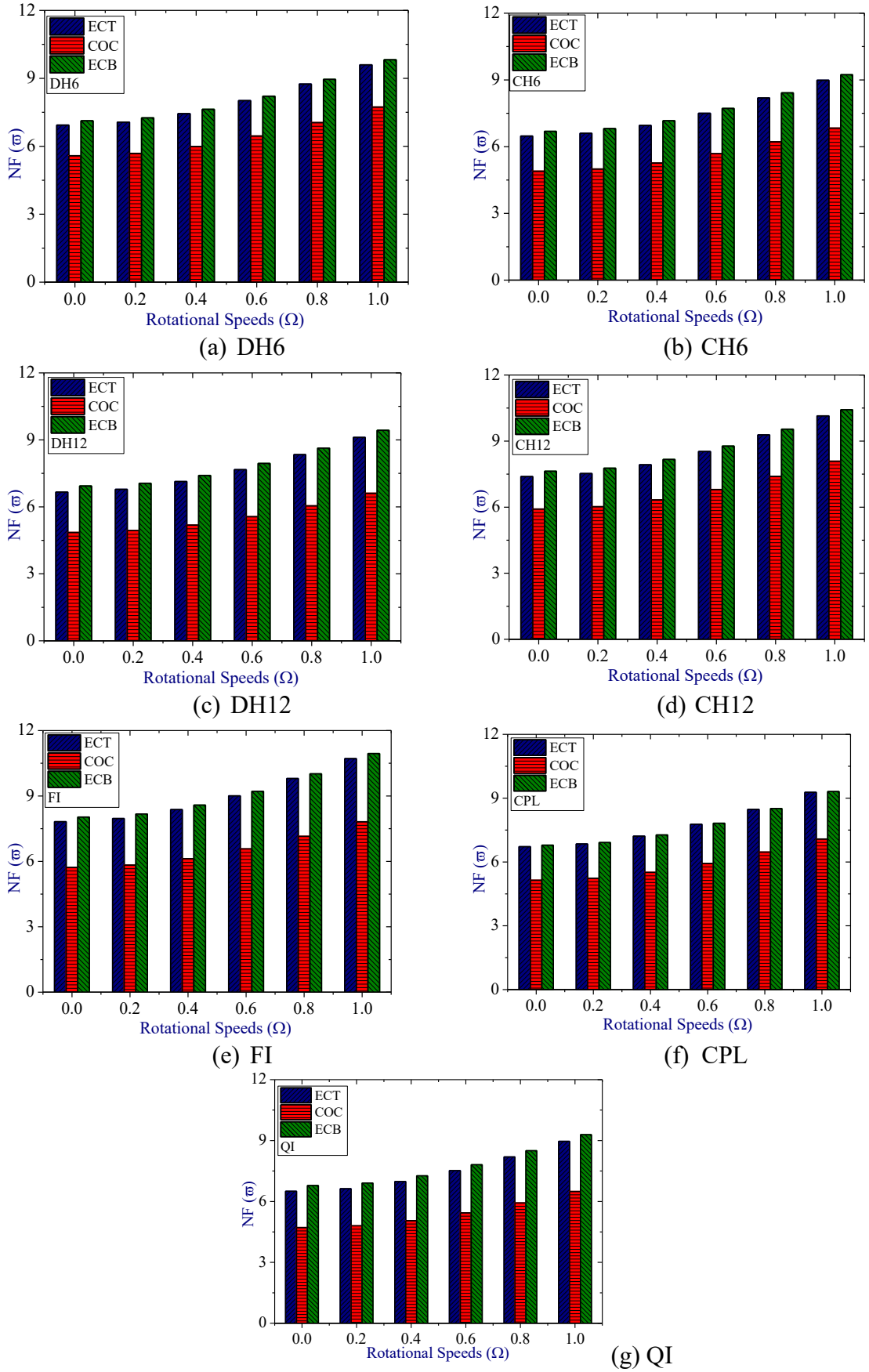


Figure 5: Influence of eccentricity on the NF of bio-inspired rotating cylindrical stiffened panels.

This results from the centrifugal force generated by spinning shells, manifesting as geometric stiffness and enhancing the fundamental frequency. The process is referred to as centrifugal stiffening.

3.1.2 Effect of stiffeners

The natural frequency of rotating bio-inspired stiffened cylinder shell panels (CYS) with stacking sequence is demonstrated in Table 7 by changing the number of stiffeners. The stiffeners are placed on the bio-inspired cylinder shell panels (CYS) along the *X* and *Y* directions, respectively. The parameters are a/b=1.0, a/h=50, R_y=10a, b_{st} =h, d_{st} =2h, λ= 0º , twist angle $\phi = 5^{\circ}$. The mass and stiffness are both improved with the addition of stiffeners in a rotating bio-inspired cylinder shell, but generally, the outcome of stiffness is a more noticeable effect than the mass. Therefore, it is evident that the addition of stiffeners to the bio-inspired cylinder shell panels (CYS) causes the FF values to increase. It is also accepted that the moments of inertia (first and second) of the structure usually improve with the addition of stiffeners to the panels. Further, it is obvious that *X*-directional stiffeners have a more pronounced influence than the *Y*-directional stiffeners. However, For CH12, CPL, and QI configurations, the negative effect of *Y*-directional stiffeners *is* identified. Fascinatingly, Among the stacking sequences, the CH12 expressed the higher values of natural frequencies due to the influences of a number of stiffeners, wherein QI (negative effect for Y directional stiffeners) exhibits the minimum values for the same analyses. It is remarkable to note that the increase in FF is steadied when more than three stiffeners are applied in both directions.

3.1.3 Effect of twist angle

In this example, the natural frequency of pre-twisted bio-inspired rotating stiffened cylindrical panels are generated by twist angle (ϕ) and shown in **Figure 6**. This study considers three sets of twist angles, such as 5°, 10°, and 15°, respectively. The parameters are as a/b =1, a/h=20, R_y=10a, b_{st} =h, d_{st} =2h, n_x=1, and n_y=1 are kept constant. It can be seen that the natural frequency (NF) values of the bio-inspired rotating stiffened cylindrical panels (CYS) decrease due to the rise in twist angle. It is possible that this is due to the fact that the value of the twisted radius of curvature, which is directly proportional to flexural rigidity, has reduced. As a result, it is exposed that the NF of the bio-inspired rotating cylindrical stiffened panels always decreases because of a rise in the pre-twist angle. Further, the natural frequency of the bio-inspired rotating stiffened cylindrical panels is always found to increase with the rise in rotational speeds (Ω). Further, it may be noted that the more effective effect of twist angle (ϕ)

is observed in DH12 configurations. In contrast, for similar analyses, the less effective effect of stiffeners is observed in QI configurations.

Table 7: The variation of FF of bio-inspired rotating stiffened cylindrical panels with several stiffeners.

Stiffeners	Mode	DH6	CH6	DH12	CH12	FI	CPL	QI
n_x=0, n_y=0	1	4.8847	4.4304	4.4411	5.7866	5.3097	4.8948	4.7080
	2	8.7077	8.0985	10.2468	11.2336	10.7189	7.3846	11.2929
	3	16.6526	26.0966	24.9406	20.2790	20.7894	29.0407	26.1295
n_x=1, n_y=0	1	6.0126	5.9382	6.0756	7.1796	7.0893	6.2850	6.3001
	2	10.2952	10.4796	12.2667	12.6541	12.3597	8.4865	13.0639
	3	17.8836	26.9700	25.5137	20.6443	21.3980	28.7745	27.3982
n_x=0, n_y=1	1	5.1474	4.5794	4.5368	5.7660	5.4036	4.8802	4.6815
	2	11.2938	10.2770	11.8765	12.8164	12.1754	8.2814	12.6074
	3	25.5868	26.9646	26.9856	29.5808	26.1476	28.6125	26.5646
n_x=1 n_y=1	1	6.5069	6.0687	6.1810	7.2233	7.3075	6.3405	6.2778
	2	12.7026	12.0676	13.5307	14.1114	13.5486	9.1755	14.1344
	3	26.1694	29.2591	30.3365	29.8497	26.5735	30.9771	31.4110
n_x=2, n_y=0	1	7.5121	7.0688	7.2863	8.2567	8.5910	7.4204	7.2032
	2	15.4295	12.5736	14.0022	14.1702	14.0817	10.0498	16.4719
	3	38.8464	31.2951	29.4002	23.9974	24.6851	29.9962	37.2207
n_x=0, n_y=2	1	7.2252	4.5483	4.5283	5.6624	5.3657	4.7867	4.5969
	2	12.0029	11.6580	12.8984	13.8472	13.0522	8.8215	13.5900
	3	21.1633	27.3473	27.2485	33.1578	31.0157	28.5588	26.6822
n_x=2 n_y=2	1	7.5121	7.0373	7.2753	8.1577	8.7281	7.3796	7.3650
	2	15.4295	14.8049	15.8908	16.3764	15.7547	10.8474	14.8200
	3	38.8464	36.6184	37.2063	40.4936	34.0301	36.2631	31.0856
n_x=3 n_y=3	1	8.2790	7.7835	8.9209	8.9209	9.8810	8.3020	7.9410
	2	17.4865	16.9523	18.2316	18.2316	17.4936	12.0261	18.4323
	3	43.6980	40.9731	45.3585	45.3585	37.9745	40.8501	41.3859
n_x=4 n_y=4	1	8.5418	8.0477	8.4747	9.2085	10.3771	8.7193	8.2330
	2	18.8411	18.2199	18.9431	19.4293	18.6802	12.8495	19.5449
	3	45.5408	42.6925	44.2375	48.0069	42.2111	43.0057	43.3838

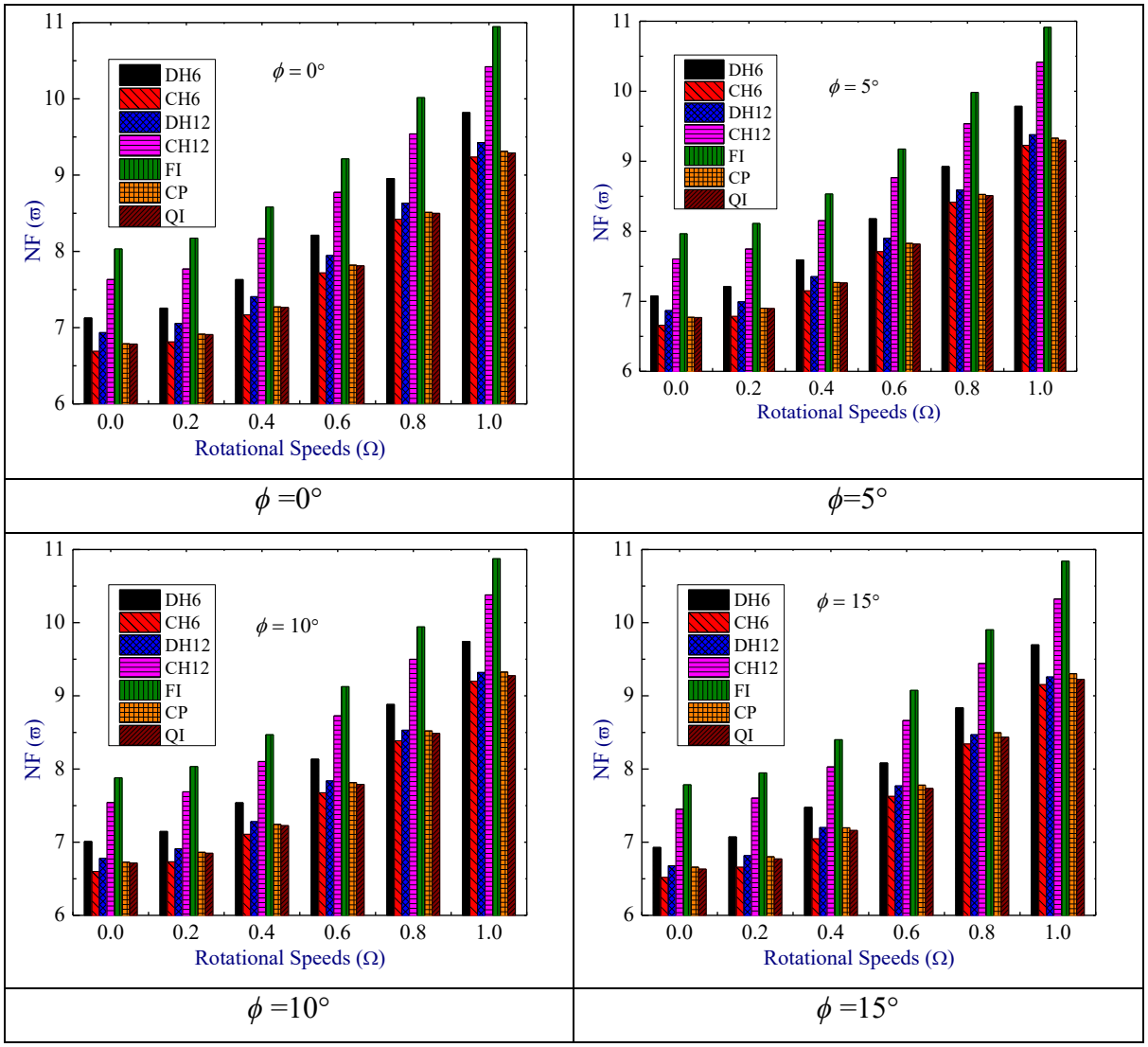


Figure 6: Influence of twist angle on the NF of bio-inspired rotating stiffened cylindrical panels

3.1.4 Effect of shallowness ratio (*Ry /a*):

The effect of shallowness ratio (*Ry /a*) on the natural frequency (NF) bio-inspired rotating cylindrical stiffened panels with the staking sequences by varying the rotational speeds are tabulated in **Table 8**. This study considers six sets of curvature ratios, including 5, 10, 15, 20, 50, and 100. The parameters are as *a/b* =1, *a/h*=20, $\phi = 5^{\circ}$, b_{st} =*h*, d_{st} =*2h*, n_x=1, and n_y=1 are kept constant. It demonstrated that the natural frequency (NF) values of the bio-inspired rotating cylindrical stiffened panels lessened due to growth in curvature ratio, regardless of rotational speeds. As expected, this trend is because the curvature effect reduces with the

increase in the shallowness ratio. From **Table 8**, As a result of the increase in rotational speeds, it has also been discovered that the greatest percentage of the increase in natural frequency occurs in the lower shallowness ratio (R_y/a = 5).

Table 8: The variation of NF of bio-inspired rotating cylindrical stiffened panels with a *R/a*.

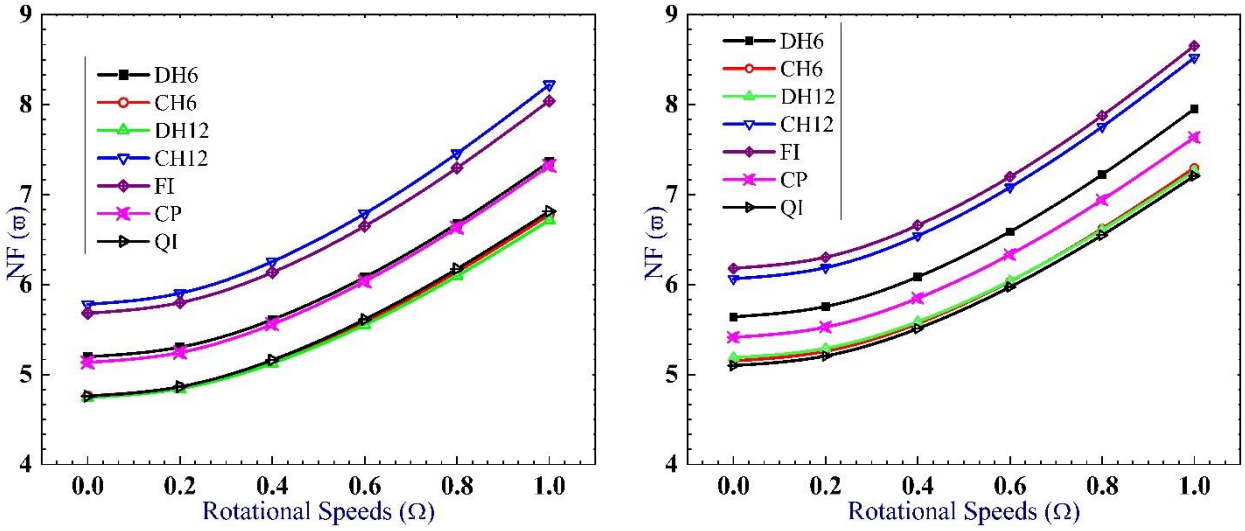
Ω	*Ry /a*	DH6	CH6	DH12	DC12	FI	CPL	QI
0.0	5	7.2349	6.8434	7.1111	7.8382	8.1727	6.8621	7.0349
	10	7.0768	6.6579	6.8687	7.6057	7.9653	6.7728	6.7690
	15	7.0358	6.6088	6.8062	7.5448	7.9145	6.7511	6.6981
	20	7.0175	6.5867	6.7786	7.5176	7.8928	6.7419	6.6662
	50	6.9886	6.5513	6.7353	7.4744	7.8601	6.7279	6.6149
	100	6.9800	6.5407	6.7227	7.4617	7.8510	6.7241	6.5996
0.25	5	7.4435	7.0431	7.3085	8.061	8.4023	7.061	7.2373
	10	7.2838	6.8559	7.0638	7.8261	8.1939	6.974	6.9686
	15	7.2428	6.8068	7.0012	7.7651	8.1436	6.9536	6.8975
	20	7.2246	6.7848	6.9737	7.7381	8.1223	6.9451	6.8656
	50	7.1961	6.7498	6.9309	7.6953	8.0904	6.9326	6.8146
	100	7.1877	6.7394	6.9185	7.6828	8.0817	6.9292	6.7994
0.5	5	8.0302	7.6033	7.8604	8.6809	9.0447	7.6134	7.7996
	10	7.8638	7.4086	7.6064	8.4369	8.8302	7.5294	7.5203
	15	7.8219	7.3586	7.5426	8.3749	8.78	7.5113	7.4475
	20	7.8037	7.3365	7.5149	8.3476	8.759	7.5042	7.4152
	50	7.7754	7.3017	7.4723	8.3051	8.7286	7.4945	7.364
	100	7.7673	7.2916	7.4602	8.2928	8.7205	7.4922	7.349
0.75	5	8.9074	8.4381	8.6795	9.5947	9.9991	8.4284	8.6269
	10	8.7267	8.2273	8.4063	9.3324	9.7694	8.3425	8.3265
	15	8.6822	8.1742	8.3389	9.267	9.717	8.3255	8.2495
	20	8.6631	8.151	8.31	9.2386	9.6955	8.3193	8.2156
	50	8.6339	8.115	8.266	9.1949	9.6651	8.3118	8.1624
	100	8.6257	8.1047	8.2536	9.1824	9.6573	8.3103	8.1469
1.0	5	9.9881	9.4637	9.6823	10.7057	11.1677	9.6311	9.4249
	10	9.7856	9.2283	9.3803	10.4164	10.9134	9.2999	9.3307
	15	9.7365	9.1697	9.3067	10.3451	10.8562	9.2159	9.3129

	20	9.7156	9.1444	9.2753	10.3144	10.833	9.1791	9.3067
	50	9.6839	9.1053	9.2279	10.2676	10.8005	9.1218	9.2999
	100	9.6751	9.0942	9.2148	10.2544	10.7924	9.1053	9.2989

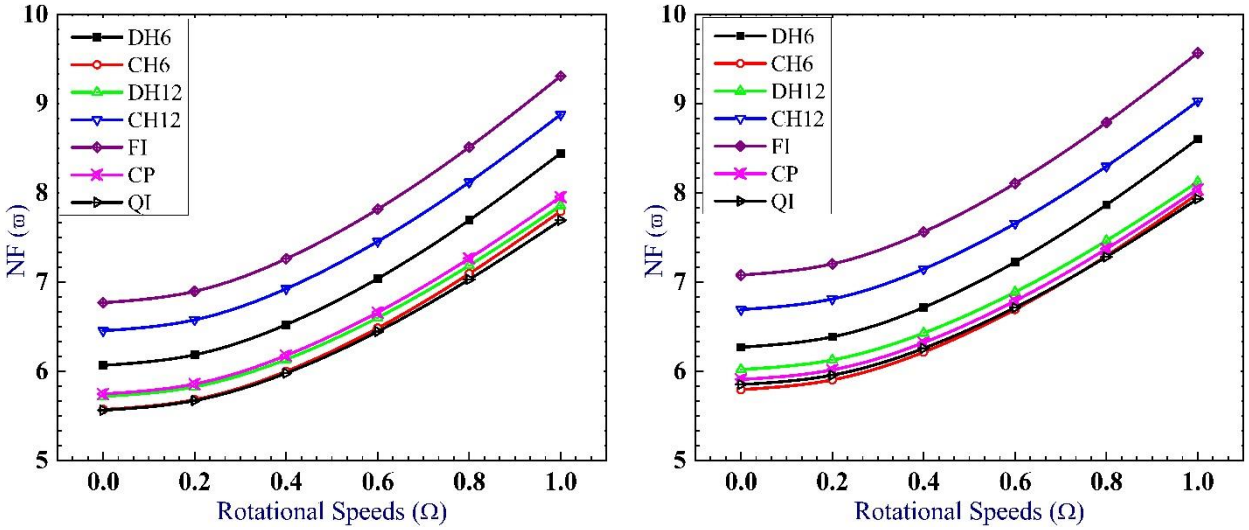
Contrary to the findings of the same investigation, the higher shallowness ratio (R_y/a = 100) is associated with the lowest percentage of rise in natural frequency. At the same time, diminishing tendencies of natural frequency are detected for bigger values of the shallowness ratio. It is obvious that the FF values of the panels increase with the rise in rotational speeds for all bio-inspired panels.

3.1.5 Effect of stiffener widths:

The effect of stiffener widths on the natural frequencies of the bio-inspired rotating cylindrical stiffened panels with stacking sequence are represented in **Figure 7** and **Figure 8**. The using parameters in this example are a/b=1.0, a/h=10, R=10a, n_x=1, n_y=1, $\phi = 5^\circ$ and d_{st} =2h. It is observed that the natural frequency increases with the increase in the stiffener width.

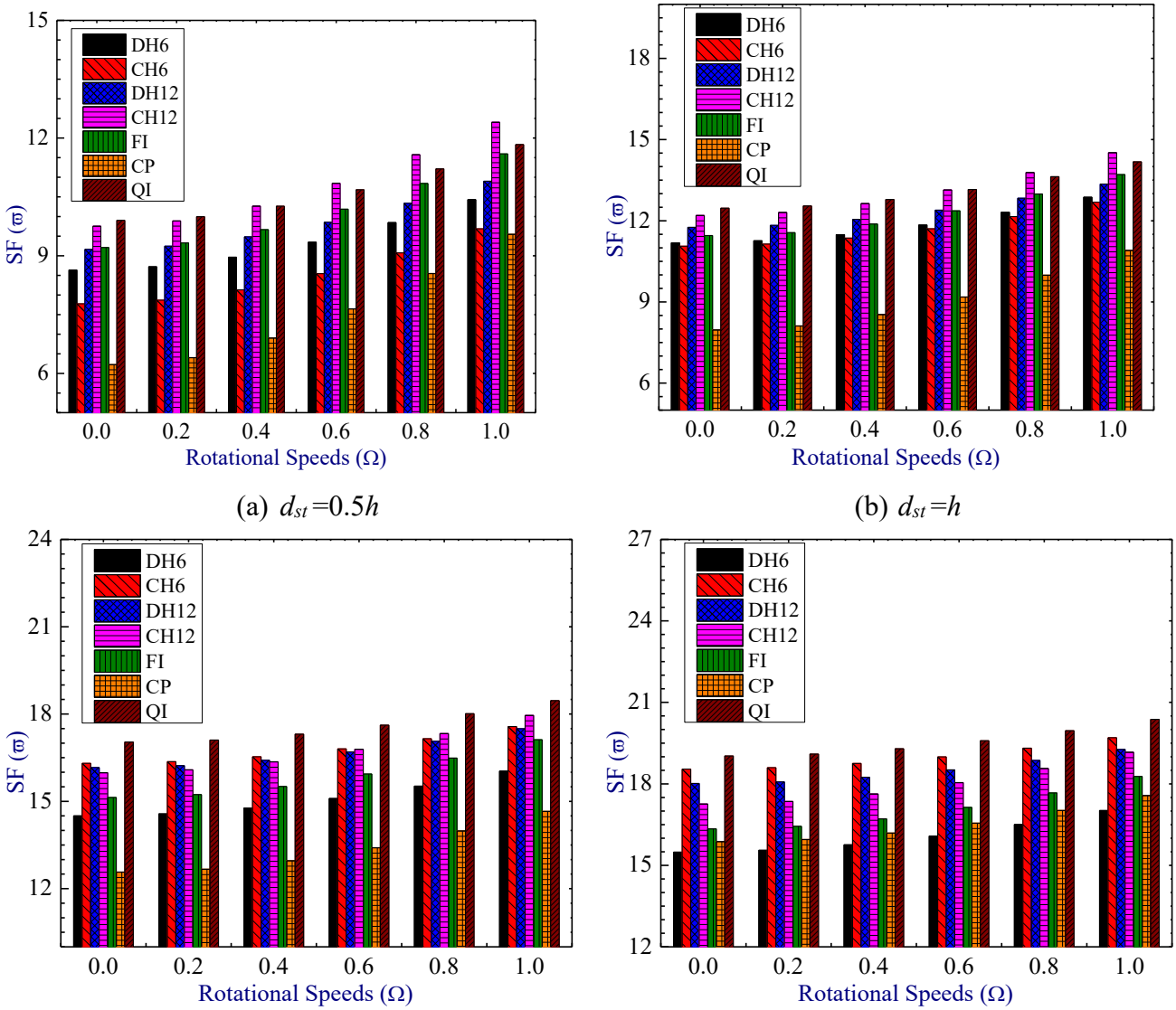


(a) d_{st}=0.5h (b) d_{st}=h



(c) $d_{st}=2h$ (d) $d_{st}=3h$

Figure 7: Influence of stiffeners width on the fundamental frequency (FF) of bio-inspired rotating stiffened cylindrical panels.

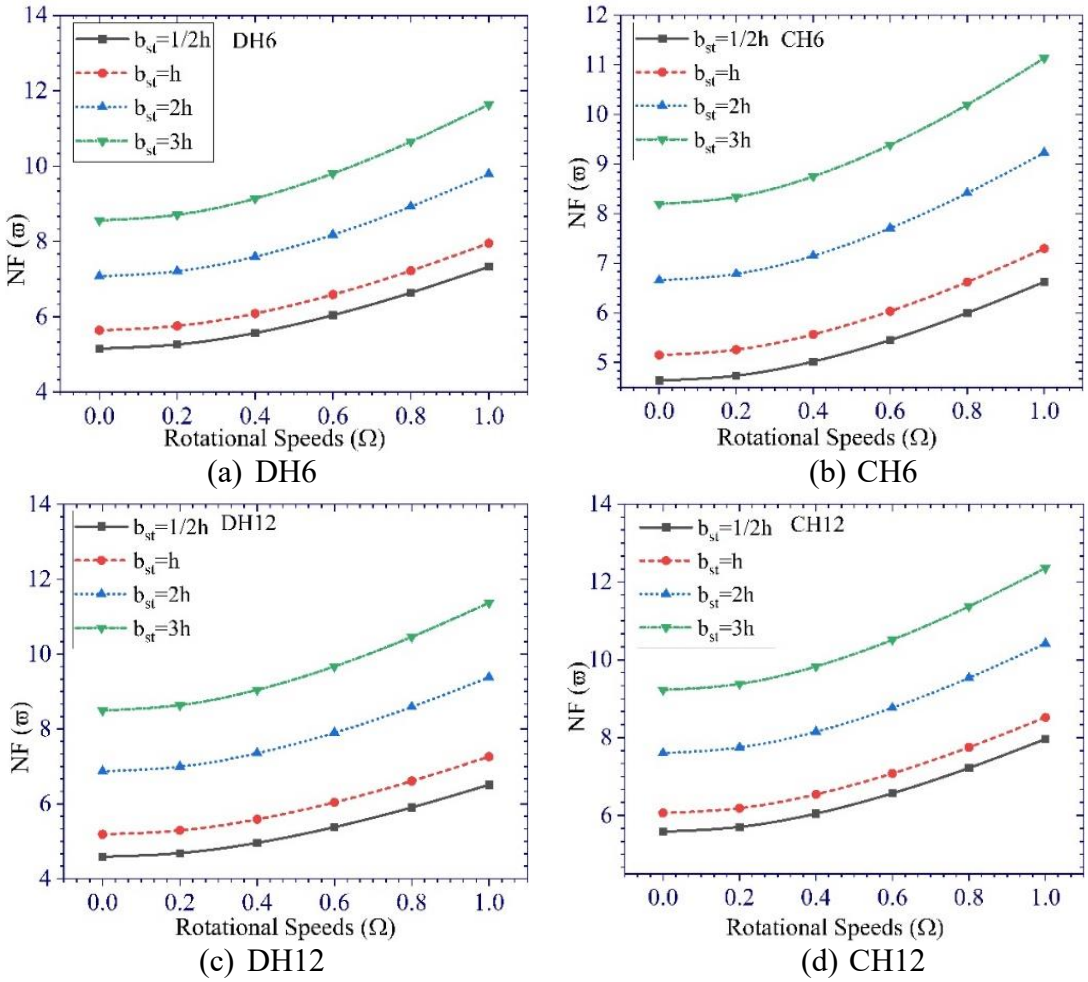


(a) $d_{st}=0.5h$ (b) $d_{st}=h$

(c) $d_{st}=2h$ (d) $d_{st}=3h$

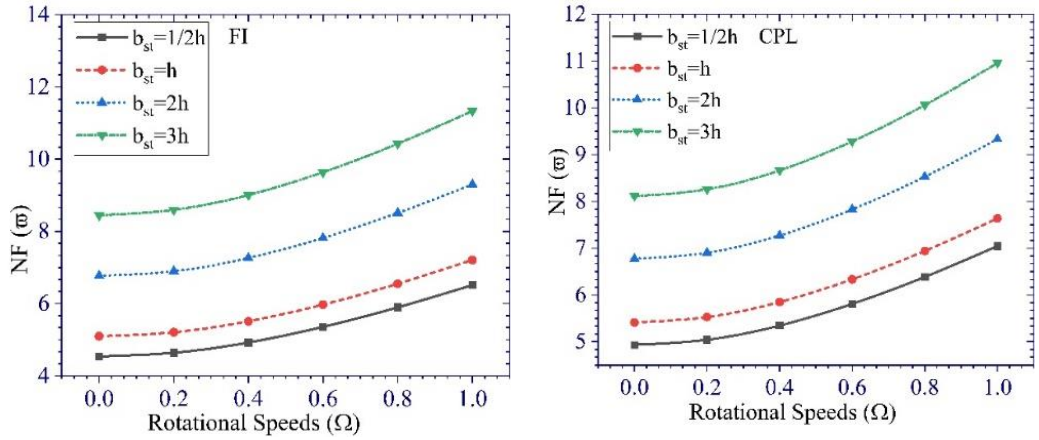
Figure 8: Influence of stiffeners width on the secondary frequency (SF) of bio-inspired rotating stiffened cylindrical panels.

It should be noticed that the DH12 type distribution has the highest percentage rise in fundamental frequency (FF) because of the rise of stiffener width, whereas the CH12 distribution exhibits the percentage rise in fundamental frequency (FF) for a similar study. This study shows that the effect of stiffener widths on the FF is more rapid growth in DH12 configurations. Interestingly, the CH6 type distribution has the highest percentage rise in fundamental frequency (FF) because of the rise of stiffener width. Further, the FI-type distribution has the minimum percentage rise in fundamental frequency (FF) because of the rise of stiffener width at stationary conditions, whereas the CPL distribution exhibits the lowest values for a similar study. It is obvious that the FF values of the panels increase with the rise in rotational speeds for all bio-inspired panels.



(a) DH6 (b) CH6

(c) DH12 (d) CH12



(e) FI (f) CPL

(g) QI

Figure 9: The effect of stiffener thickness on the natural frequency of the bio-inspired rotating stiffened cylindrical panels.

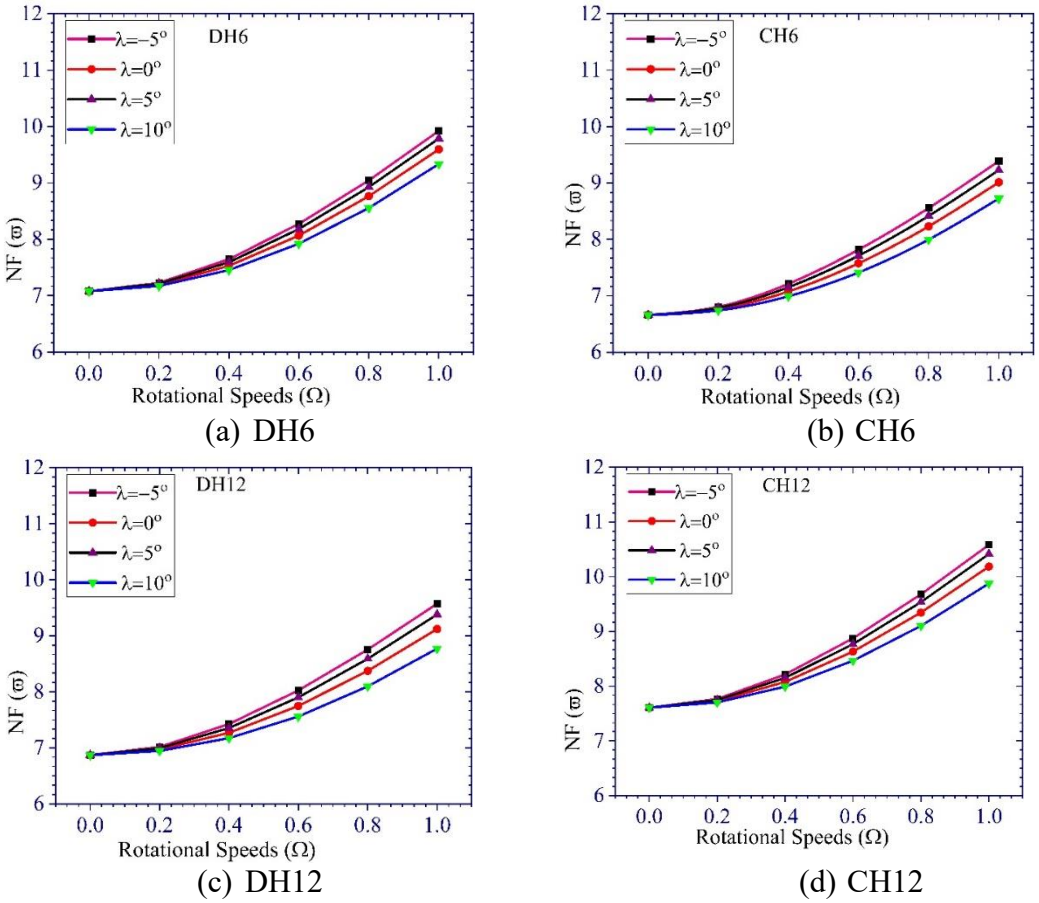
3.1.6 Effect of stiffeners thickness:

The influence of stiffener thickness on the natural frequencies of the bio-inspired spinning cylindrical stiffened panels with stacking sequence is described in **Figure 9**. The parameters used in this example are a/b=1.0, a/h=20, R=10a, n_x=1, n_y=1 $\phi = 5^\circ$, and d_{st} =h. It is observed that the natural frequency intensifications with the increase in the stiffener thickness. It is obvious that the DH12 type distribution has the highest percentage rise in fundamental frequency (FF) because of the rise of stiffener thickness, irrespective of rotational speeds. This study indicates that the effect of stiffener thickness on the NF is more rapid growth in DH12 configurations. Fascinatingly, the CH6 type distribution has a minimal percentage rise in fundamental frequency (FF) because of the rise of stiffener thickness. Further, the DH6 type distribution has the minimum percentage rise in fundamental frequency (FF) because of the rise of stiffener thickness at stationary conditions, whereas the CH6 distribution exhibits the minimum percentage rise in fundamental frequency (FF) at full rotational conditions. It is

obvious that the FF values of the panels increase with the rise in rotational speeds for all bio-inspired panels.

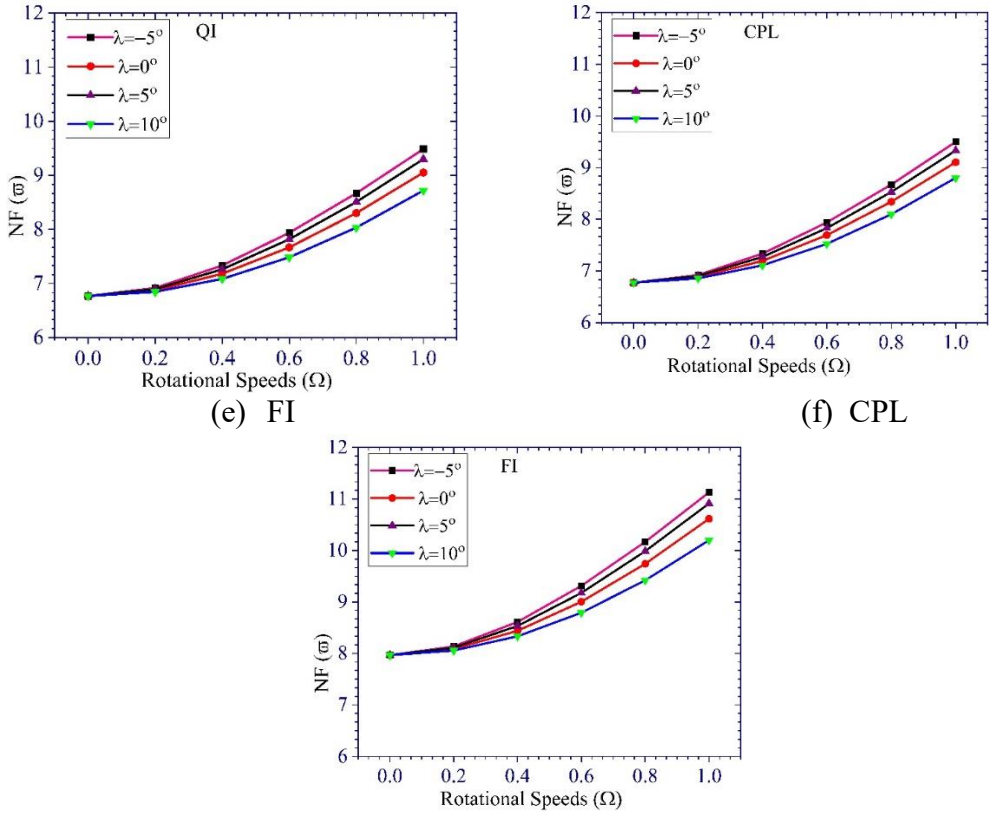
3.1.7 Effect of Pre-cone angle (λ):

Figure 10 illustrates the impact of pre-cone angle (λ) on the natural frequency values (FF) of bio-inspired rotating stiffened CYS panels with stacking sequences. The natural frequency outcomes are plotted against the non-dimensional rotational speeds (**Ω**). The parameters, a/b=1, a/h = 20, R_y/a =5, $\phi = 5^\circ$, b_{st} =h, d_{st} =$2h$, n_x=1, and n_y=1 are keep up constant. Whereas, the impact of the pre-cone angle (λ) is more noticeable at higher values of **Ω** as expected. Fascinatingly, it has been recognized that the frequency values of the panels are reduced with the increase in the pre-cone angle (λ) and its effect on the frequency is slightly downward when the **Ω** value is increased. Interestingly, a higher percentage downfall of FF is observed with the CH12 configuration, whereas minimal effect is found with the DH6 configuration. Furthermore, the impact of the pre-cone angle is consistently increased as the rotational speeds (**Ω**) rise. It is obvious that the FF values of the panels increase with the rise in rotational speeds for all bio-inspired panels.



(a) DH6 (b) CH6

(c) DH12 (d) CH12



(e) FI (f) CPL

(g) QI

Figure 10: Effect of pre-cone angle (λ) on the FF of bio-inspired rotating cylindrical stiffened panels.

3.1.8 Mode Shape:

The consequence of stacking sequence on the first four mode shape of bio-inspired rotating cylindrical stiffened panels is depicted in **Table 9** with stationary conditions and **Table 10** with rotational speeds, respectively. The black nodal lines indicate points of zero displacement. The initial four modes of DH6 and CH6 are identified as spanwise bending (1B), torsion (1T), chordwise bending (1C), and a combination of bending and torsion (1BT), respectively. The initial four modes of DH12 are spanwise bending (1B), torsion (1T), secondary spanwise bending (2B), and a combination of bending and torsion (1BT), respectively. The initial four modes of DH12 are spanwise bending (1B), torsion (1T), secondary torsion (1T), and secondary spanwise bending (2B), respectively. The initial four modes of FI and CPL are spanwise bending (1B), torsion (1T), chordwise bending (1C), and combinations of chordwise bending (1C) and spanwise bending (2B), respectively. The initial four modes of QI are spanwise bending (1B), torsion (1T), chordwise bending (1C), and second chordwise bending (2C), respectively. Interestingly, the significant effect of rotational speeds is recognised on the mode shapes. Further the nodal displacements are comparably less in rotational conditions.

Table 9: The first four mode shape of bio-inspired rotating cylindrical stiffened panels with a stacking sequence at Ω=0.

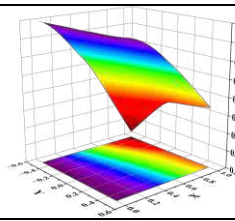
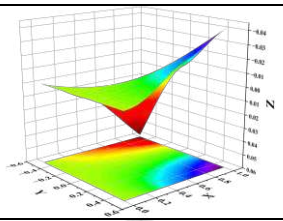
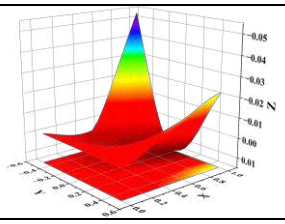
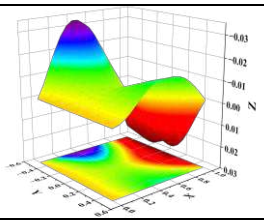
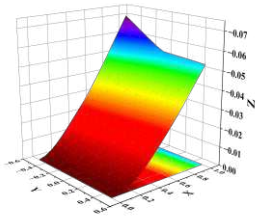
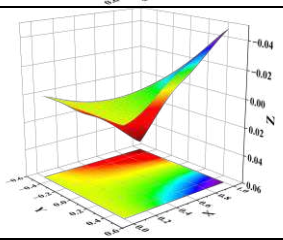
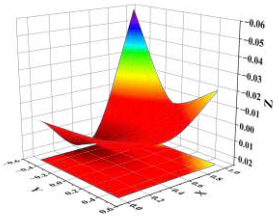
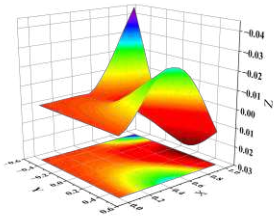
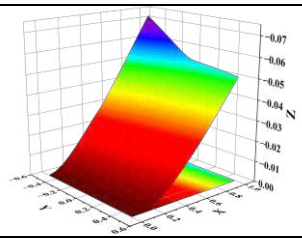
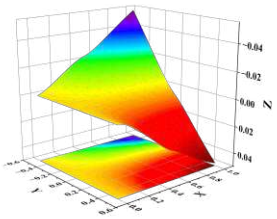
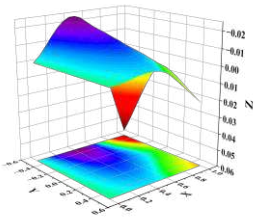
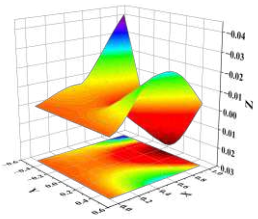
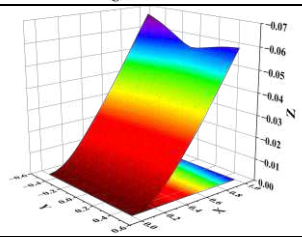
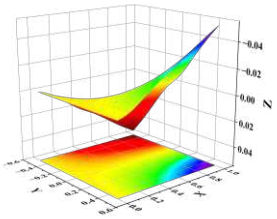
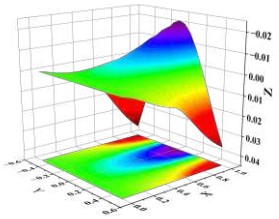
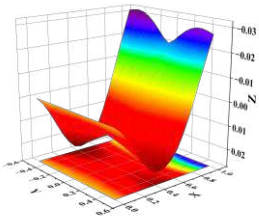
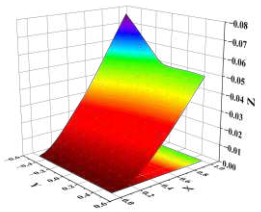
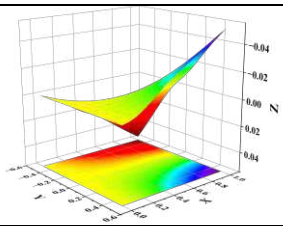
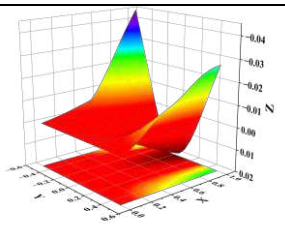
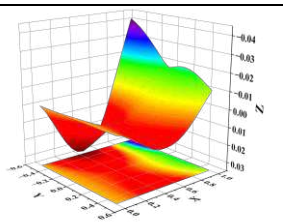
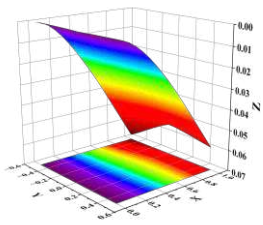
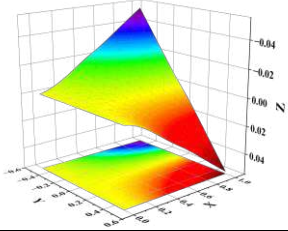
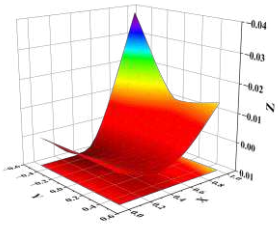
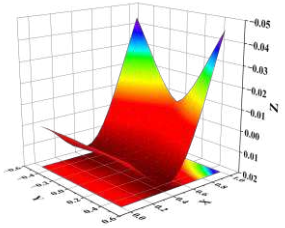
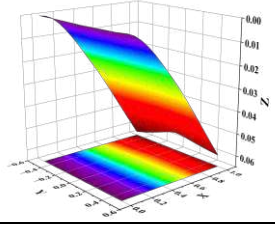
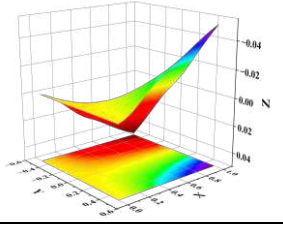
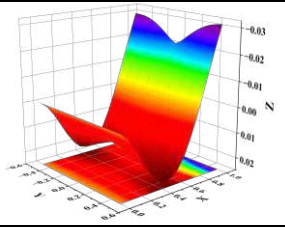
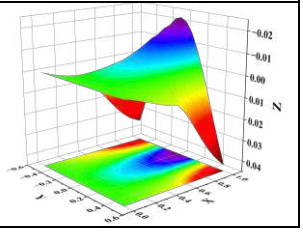
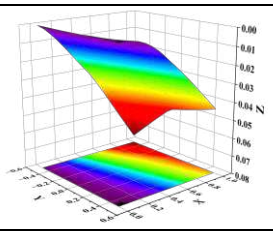
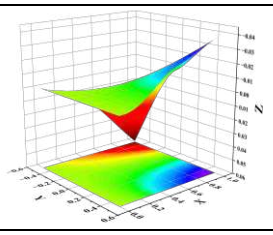
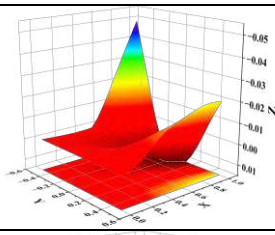
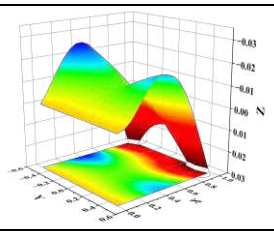
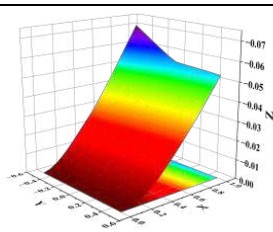
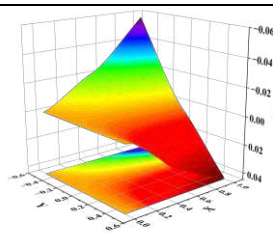
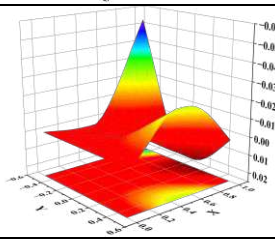
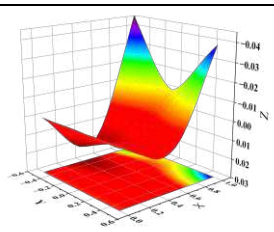
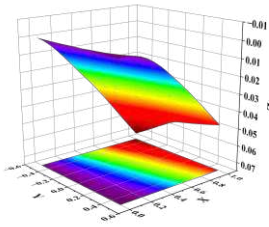
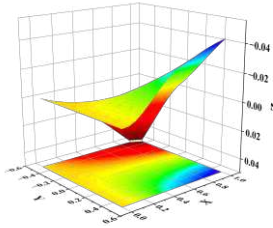
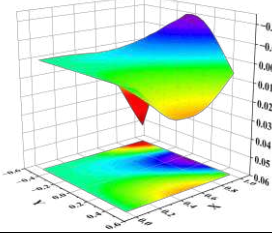
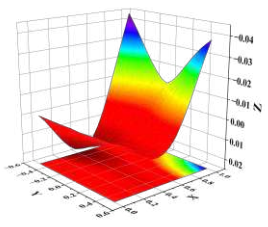
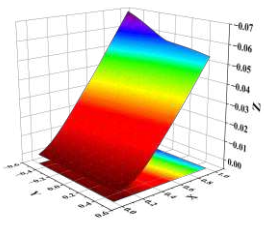
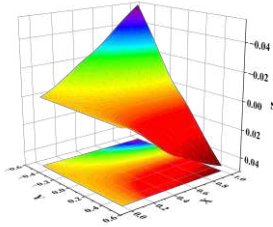
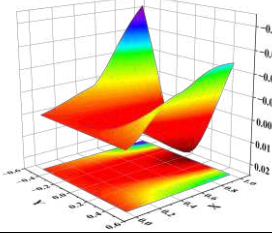
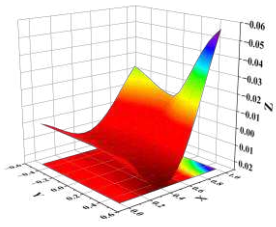
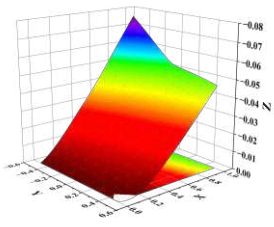
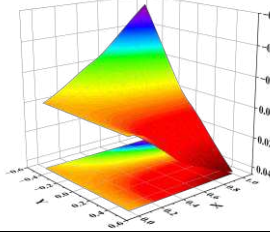
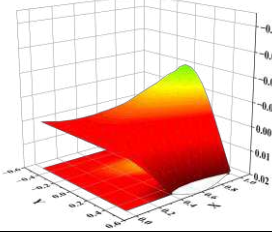
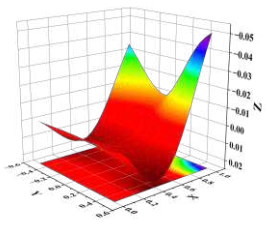
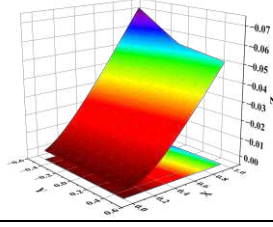
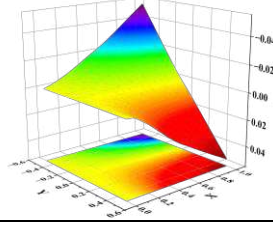
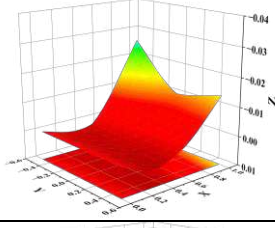
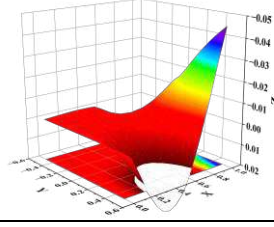
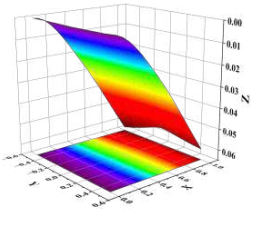
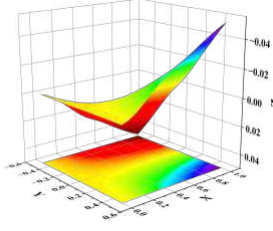
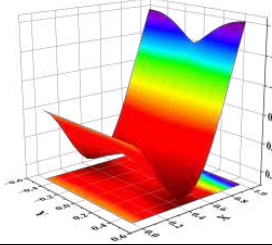
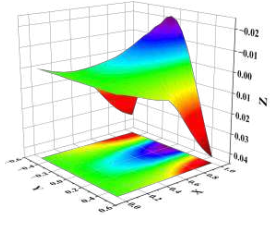
Θ	1st Mode	2nd Mode	3rd Mode	4th Mode
DH6				
CH6				
DH12				
CH12				
FI				
CPL				
QI				

Table 10: The first mode shape of bio-inspired rotating cylindrical stiffened panels with a stacking sequence at **Ω**=1.0.

Θ	1st Mode	2nd Mode	3rd Mode	4th Mode
DH6				
CH6				
DH12				
CH12				
FI				
CPL				
QI				

3.1.9 Conclusions:

The finite element analysis (FEM) is used to look at the free vibration behaviour of stiffened rotating cylindrical shells. The geometry of the bio-inspired rotating stiffened cylindrical panels is modelled based on the first-order shear deformation theory (FSDT). In the process of modelling the stiffener, three nodded curved isoparametric beam elements are utilized. These elements have four degrees of freedom, which include two translations and two rotations. For the purpose of the stiffener, a rectangular section composed of graphene-reinforced composite materials with a constant width (b_{st}) and depth (d_{st}) is being evaluated. The validations have shown that the current formulation is accurate. In this present research, seven different stacking sequences are taken into consideration along with various geometric parameters like length (a), width (b), curvature ratios (R_y/a), uniform thickness (h), the radius of curvature (R_y), twist angle (ϕ), the effect of stiffeners, the effect of eccentricity and rotational speeds. A summary of the most important findings is provided below.

1. It is evident that the addition of stiffeners to the bio-inspired rotating cylindrical stiffened panels causes the NF values to increase.
2. It is interesting that the maximum values of natural frequency are identified when stiffeners are placed eccentric at bottom (ECB) and minimum when stiffeners are concentric (COC).
3. It can be seen that the NF values of the bio-inspired rotating cylindrical stiffened panels decrease due to the rise in twist angle, while the natural frequency of the bio-inspired rotating cylindrical stiffened panels always is found to increase rate due to rise in rotational speeds.
4. It demonstrated that the NF values of the bio-inspired rotating cylindrical stiffened panels decrease due to a rise in shallowness ratio.
5. It can be seen that the NF values of the bio-inspired rotating cylindrical stiffened panels increase due to the rise in stiffeners with and thickness. Moreover, it is clearly seen that the stiffener's thickness has a more significant performance than the width of the stiffeners having the same weight.
6. It has been recognized that the frequency values of the panels are reduced with the increase in the pre-cone angle (λ), and its effect on the frequency is slightly downward when the **Ω** value is increased.

7. The consequence of stacking sequence on the first mode shape of bio-inspired rotating cylindrical stiffened panels is depicted with stationary conditions and with rotational speeds, respectively.

4 References

[1] Sosinka A, Rost-Roszkowska MM, Vilimova J, Tajovský K, Kszuk-Jendrysik M, Chajec T, et al. The ultrastructure of the midgut epithelium in millipedes (Myriapoda, Diplopoda). Arthropod Struct Dev 2014;43:477–92. https://doi.org/10.1016/j.asd.2014.06.005.

[2] Chen J, Xie J, Wu Z, Elbashiry EMA, Lu Y. Review of beetle forewing structures and their biomimetic applications in China: (I) on the structural colors and the vertical and horizontal cross-sectional structures. Mater Sci Eng C 2015;55:605–19. https://doi.org/10.1016/j.msec.2015.05.064.

[3] Tuo W, Chen J, Wu Z, Xie J, Wang Y. Characteristics of the tensile mechanical properties of fresh and dry forewings of beetles. Mater Sci Eng C 2016;65:51–8. https://doi.org/10.1016/j.msec.2016.04.025.

[4] Sharma A, Belarbi MO, Garg A, Li L. Bending analysis of bio-inspired helicoidal/Bouligand laminated composite plates. Mech Adv Mater Struct 2024;31:5326–40. https://doi.org/10.1080/15376494.2023.2214934.

[5] Li B, Hong J, Yan S, Liu Z. Multidiscipline topology optimization of stiffened plate/shell structures inspired by growth mechanisms of leaf veins in nature. Math Probl Eng 2013;2013. https://doi.org/10.1155/2013/653895.

[6] Shang JS, Ngern NHH, Tan VBC. Crustacean-inspired helicoidal laminates. Compos Sci Technol 2016;128:222–32. https://doi.org/10.1016/j.compscitech.2016.04.007.

[7] van de Kamp T, Riedel A, Greven H. Micromorphology of the elytral cuticle of beetles, with an emphasis on weevils (Coleoptera: Curculionoidea). Arthropod Struct Dev 2016;45:14–22. https://doi.org/10.1016/j.asd.2015.10.002.

[8] Meyers MA, Chen PY, Lin AYM, Seki Y. Biological materials: Structure and mechanical properties. Prog Mater Sci 2008;53:1–206. https://doi.org/10.1016/j.pmatsci.2007.05.002.

[9] Sun CT, Chen JK. On the Impact of Initially Stressed Composite Laminates. J Compos Mater 1985;19:490–504. https://doi.org/10.1177/002199838501900601.

[10] Sahoo S. Laminated composite stiffened shallow spherical panels with cutouts under free vibration – A finite element approach. Eng Sci Technol an Int J 2014;17:247–59.

https://doi.org/10.1016/j.jestch.2014.07.002.

[11] Maji P, Rout M, Karmakar A. The thermo-elastic vibration of graphene reinforced composite stiffened plate with general boundary conditions. Structures 2021;33:99–112. https://doi.org/10.1016/j.istruc.2021.04.029.

[12] Mouthanna A, Bakhy SH, Al-Waily M. Analytical Investigation of Nonlinear Free Vibration of Porous Eccentrically Stiffened Functionally Graded Sandwich Cylindrical Shell Panels. Iran J Sci Technol - Trans Mech Eng 2023;47:1035–53. https://doi.org/10.1007/s40997-022-00555-4.

[13] Zhou Y, Zhang Y, Nyasha Chirukam B, Li J, Lu C, Babaei M, et al. Free Vibration Analyses of Stiffened Functionally Graded Graphene-Reinforced Composite Multilayer Cylindrical Panel. Mathematics 2023;11. https://doi.org/10.3390/math11173662.

[14] Maji P, Rout M, Karmakar A. The free vibration response of temperature-dependent carbon nanotube-reinforced composite stiffened plate. Mech Adv Mater Struct 2021;0:1–15. https://doi.org/10.1080/15376494.2020.1870782.

[15] Duc ND. Nonlinear dynamic response of imperfect eccentrically stiffened FGM double curved shallow shells on elastic foundation. Compos Struct 2013;99:88–96. https://doi.org/10.1016/j.compstruct.2012.11.017.

[16] Yang Y, Ye T, LI S, Jin G, Chen Y, Zhong S. A semi-analytical method for vibro-acoustic characteristics of orthogonal stiffened laminated cylindrical shells. J Sound Vib 2023;558:117770. https://doi.org/10.1016/j.jsv.2023.117770.

[17] Gao C, Pang F, Li H, Huang X, Liang R. Prediction of vibro-acoustic response of ring stiffened cylindrical shells by using a semi-analytical method. Thin-Walled Struct 2024;200:111930. https://doi.org/10.1016/j.tws.2024.111930.

[18] Reddy JN LC. A higher-order shear deformation theory of laminated elastic shells. Int J Eng Sci 1985;23:319–30.

[19] Karmakar A KK. Free Vibration Analysis of Delaminated Composite Pretwisted Rotating Shells─ A Finite Element Approach. JSME Int J Ser A Solid Mech Mater Eng 2006;49:492–502.

[20] Sreenivasamurthy S R V. Coriolis effect on the vibration of flat rotating low aspect ratio cantilever plates. He J Strain Anal Eng Des 1981;16:97–106.

[21] Qatu, MS , Leissa A. Natural frequencies for cantilevered doubly-curved laminated composite shallow shells. Compos Struct 1991;17:227–55.

[22] Guo W, Hong X, Luo W, Yang J, Li T, Zhu X. Vibration analysis of conical–cylindrical–spherical shells by a novel linear expression method. Compos Struct 2024;334:117879.

https://doi.org/10.1016/j.compstruct.2024.117879.

[23] Jahanbazi R, Kiani Y, Beni YT. Free vibration behaviour of composite laminated skew cylindrical shells reinforced with graphene platelets. Structures 2024;61:106074. https://doi.org/10.1016/j.istruc.2024.106074.

[24] Maji P, Singh BN. Shear deformation theory for free vibration responses of 3D braided pre-twisted conical shells under rotation. Int J Comput Methods Eng Sci Mech 2021;0:1–20. https://doi.org/10.1080/15502287.2021.1916792.

[25] Maji P, Singh BN. Free vibration responses of 3D braided rotating cylindrical shells based on third-order shear deformation. Compos Struct 2020;260:113255. https://doi.org/10.1016/j.compstruct.2020.113255.

[26] Maji P, Rout M, Karmakar A. Free vibration response of carbon nanotube reinforced pretwisted conical shell under thermal environment. Proc Inst Mech Eng Part C J Mech Eng Sci 2020;234:770–83. https://doi.org/10.1177/0954406219886325.

[27] Pabitra Maji, Mrutyunjay Rout AK. Free vibration analysis of cnts-reinforced functionally graded conical shell. Int. J. Mech. Prod. Eng. Res. Dev., vol. 5, 2018, p. 25–32. https://doi.org/10.1016/j.matpr.2018.03.012.

[28] Rout M, Bandyopadhyay T, Karmakar A. Free vibration analysis of pretwisted delaminated composite stiffened shallow shells: A finite element approach. J Reinf Plast Compos 2017;36:619–36. https://doi.org/10.1177/0731684416689726.

[29] Zhang C, Liu P, Zhu D, Van Lich L, Bui TQ. Analysis of natural frequency for bioinspired functional gradient plates. Int J Mech Mater Des 2020;16:367–86. https://doi.org/10.1007/s10999-019-09466-w.

[30] Dhari RS, Patel NP, Wang H, Hazell PJ. Numerical investigation of Fibonacci series based bio-inspired laminates under impact loading. Compos Struct 2021;255:112985. https://doi.org/10.1016/j.compstruct.2020.112985.

[31] Mohamed SA, Mohamed N, Eltaher MA. Bending, buckling and linear vibration of bio-inspired composite plates. Ocean Eng 2022;259:111851. https://doi.org/10.1016/j.oceaneng.2022.111851.

[32] Ouyang W, Wang H, Dong J, Gong B, Scarpa F, Peng HX. Cross-helicoidal approach to the design of damage-resistant composites. Compos Struct 2023;306:116577. https://doi.org/10.1016/j.compstruct.2022.116577.

[33] Do NT, Nguyen TT, Tran TT, Le PB, Pham QH. Free vibration analysis of bio-inspired helicoid laminated composite plates resting on elastic foundation using isogeometric analysis and artificial neural network. Mech Time-Dependent Mater 2023.

https://doi.org/10.1007/s11043-023-09649-1.

[34] Garg A, Li L, Sharma A. Free vibration analysis of bio-inspired double- and cross-helicoidal laminated composite plates. Mech Based Des Struct Mach 2024. https://doi.org/10.1080/15397734.2024.2357755.

[35] Kiran R, Singh D, Singh SK, Saini A, Song Y, Vaish R. On the isogeometric analysis of vibration and buckling of bioinspired composite plates using inverse hyperbolic shear deformation theory. Mech Based Des Struct Mach 2024;0:1–38. https://doi.org/10.1080/15397734.2024.2378474.

[36] Sobhani Aragh B, Tan W, Borzabadi Farahani E, Al-Greer M, Hughes D. Porosity-dependent stability analysis of bio-inspired cellular nanocomposite shells. Int J Mech Sci 2024;263:108763. https://doi.org/10.1016/j.ijmecsci.2023.108763.

[37] Mencattelli L, Pinho ST. Realising bio-inspired impact damage-tolerant thin-ply CFRP Bouligand structures via promoting diffused sub-critical helicoidal damage. Compos Sci Technol 2019;182:107684. https://doi.org/10.1016/j.compscitech.2019.107684.

[38] Eltaher MA, Aleryani OA, Melaibari A, Abdelrahman AA. Bending and Vibration of a Bio-inspired Bouligand Composite Plate Using the Finite-Element Method. Mech Compos Mater 2024;59:1199–216. https://doi.org/10.1007/s11029-023-10166-y.

[39] Garg A, Li L. Data-driven uncertainty quantification and sensitivity studies in free vibration behavior of bio-inspired helicoidal laminated composite cylindrical shells. Mech Adv Mater Struct 2024. https://doi.org/10.1080/15376494.2024.2355369.

[40] Karamanli A, Vo TP, Eltaher MA. Comprehensive analysis of bio-inspired laminated composites plates using a quasi-3D theory and higher order FE models. Thin-Walled Struct 2024;198:111735. https://doi.org/10.1016/j.tws.2024.111735.

[41] Tran Thi Thu T, Nguyen Anh T, Nguyen Thi H, Nguyen Thi H. Transient response of doubly-curved bio-inspired composite shells resting on viscoelastic foundation subject to blast load using improved first-order shear theory and isogeometric approach. Def Technol 2024;38:171–93. https://doi.org/10.1016/j.dt.2024.02.003.

[42] Daniel R C, Sudhagar PE. Vibration analysis of bio-inspired sandwich composite beam under rotating environment based on the Internet of Things technology. Mech Based Des Struct Mach 2024;52:8569–609. https://doi.org/10.1080/15397734.2024.2323151.

[43] Tao T, Li L, He Q, Wang Y, Guo J. Mechanical Behavior of Bio-inspired Honeycomb–Core Composite Sandwich Structures to Low-Velocity Dynamic Loading. Materials (Basel) 2024;17. https://doi.org/10.3390/ma17051191.

[44] Maji P, Rout M, Karmakar A. Free vibration response of carbon nanotube reinforced

pretwisted conical shell under thermal environment. Proc Inst Mech Eng Part C J Mech Eng Sci 2020;234. https://doi.org/10.1177/0954406219886325.

[45] Cook RD. Concepts and applications of finite element analysis. 2007.

[46] Ferreira AJM. MATLAB codes for finite element analysis. 2009.

Appendix

$$\left[T_{\theta x}\right]^T = \begin{bmatrix} 1 & 0 & 0 \\ 0 & \cos\chi & -\sin\chi \\ 0 & \sin\chi & \cos\chi \end{bmatrix} \qquad \left[T_{\theta y}\right]^T = \begin{bmatrix} \cos\lambda & 0 & -\sin\lambda \\ 0 & 1 & 0 \\ \sin\lambda & 0 & \cos\lambda \end{bmatrix}$$

$$\left[A_1\right] = \begin{bmatrix} 0 & -2\Omega'_z & 2\Omega'_y \\ 2\Omega'_z & 0 & -2\Omega'_x \\ -2\Omega'_y & 2\Omega'_x & 0 \end{bmatrix} \qquad \left[A_2\right] = \begin{bmatrix} \Omega'^2_y + \Omega'^2_z & -\Omega'_x\Omega'_y & -\Omega'_x\Omega'_z \\ -\Omega'_x\Omega'_y & \Omega'^2_x + \Omega'^2_z & -\Omega'_y\Omega'_y \\ -\Omega'_x\Omega'_z & -\Omega'_y\Omega'_z & \Omega'^2_x + \Omega'^2_y \end{bmatrix}$$

$$\left[T_{sx}\right] = \begin{bmatrix} 1 & 0 & 0 & e & 0 \\ 0 & 0 & 1 & 0 & 0 \\ 0 & 0 & 0 & 1 & 0 \\ 0 & 0 & 0 & 0 & 1 \end{bmatrix}$$